Construction and Building Materials 544 (2026) 148327

Contents lists available at ScienceDirect

Construction and Building Materials

journal homepage: www.elsevier.com/locate/conbuildmat

Mechanical characterization of Eastern Canada's field-extracted old clay brick masonry constituents and assemblies via experimental testing

L. Davis [a,*], W. Garcia Mendez [a], M.J. Nollet [b], D. Malomo [a]

[a] Department of Civil Engineering, McGill University, 817 Sherbrooke Street West, Montréal, QC, H3A 0C3, Canada
[b] Department of Construction Engineering, École de technologie supérieure, 1100 R. Notre Dame O, Montréal, QC, H3C 1K3, Canada

ARTICLE INFO

Keywords:
Unreinforced masonry
Triplet testing
Experimental testing
Uniaxial compression
Shear-compression
Extracted samples

ABSTRACT

Canada is one of the few earthquake-prone countries worldwide without a performance-based building code, partly because of lacking reference mechanical values for its existing structures. This is particularly concerning for Eastern Canada's unreinforced masonry (URM), whose constituent- and assembly-scale mechanical behaviour is mostly still unknown. This work is the first in Canada to quantify experimentally, in controlled conditions, the uniaxial compression or shear-compression (referred to simply as *shear* hereinafter) responses of 19th-20th century field-extracted clay brick URM constituents (bricks, mortars) and assemblies (mortared brick masonry prisms) – essential yet previously missing data for conducting informed structural assessments. First, masonry constituents are tested individually to infer physical, elastic and plastic properties using compression tests of bricks and double punch tests of mortars. Then, under uniaxial compression (ASTM C1314), masonry assemblies were subjected to monotonic or cyclic loading for measuring Young's modulus (680–2740 MPa), strength (4.2–14.1 MPa) and compression fracture energy (17.3–65.2 N/mm^2) parameters – mixed joint-brick failures were often observed. Shear tests (EN 1052–3) were conducted on masonry assemblies at three distinct levels of precompression (0.2, 0.6, 1.0 MPa), yielding shear modulus (341–626 MPa), friction coefficient (0.44–0.69), dilatancy (1.3–30.6) and cohesion (0.1–0.2 MPa), as well as Mode II fracture energy (0.07–0.49 Nmm/mm^2), exhibiting behaviours mostly governed by dry friction and joint sliding. This paper also provides first recommendations for predictive equations useful in design, including a shear/Young's modulus ratio, a correlation equation between masonry Young's modulus and compressive strength and an equation estimating masonry compressive strength using constituent values.

1. Introduction

Experimentally quantifying the mechanical properties of existing unreinforced masonry (URM) remains an important and often difficult step in the preservation of existing buildings. In e.g. Europe [1–5] and New Zealand [6–8], decades of research and URM characterization campaigns have led to robust databases of reference properties and reliable design guidelines, as well as leading performance-based building code provisions (e.g. Eurocodes, NZSEE). In North America, beyond ASCE 41–23 (which bases most of its information on European studies or older local construction manuals) reference mechanical data on existing URM are still largely missing. Canada lags further behind, despite the prevalence of URM in urban centres, given the absence of data-driven guidelines on the structural features of its traditional URM – adapted in unique ways by European settlers to fit local resources and the cold climate [9]. The unwanted cascade effects of this chronic lack of knowledge dramatically increases design penalties through unfavourable confidence factors, leading to overdesign and unbearably high projected renovation costs. Thus Canada has, in fact, some of the highest rates of old building demolitions worldwide [10]. Guidance provided in the National Building Code of Canada (NBCC) and provincial amendments remains limited (e.g. Commentary L), leaving engineering professionals and researchers without clear direction. National guidelines on the evaluation of old URM buildings were published in the 1990s by National Resources Canada (NRC) and focused on seismic screening (NRC 1993a), evaluation (NRC 1993b) and upgrading (NRC 1995) approaches, complemented by newly released editions [11] focused on a tiered assessment methodology for existing buildings (not necessarily URM compatible) with performance-based frameworks. Such advances will hardly be fully exploitable for local URM, as building archetype

* Corresponding author.
E-mail address: lucy.davis@mail.mcgill.ca (L. Davis).

https://doi.org/10.1016/j.conbuildmat.2026.148327
Received 2 July 2026; Received in revised form 8 September 2026; Accepted 22 September 2026
Available online 30 September 2026
0950-0618/© 2026 The Author(s). Published by Elsevier Ltd. This is an open access article under the CC BY-NC-ND license (http://creativecommons.org/licenses/by-nc-nd/4.0/).

classifications refer to ASCE 41–23 and are not representative of Canada's building stock, wherein reference characteristics of URM materials/assemblies are either missing or taken from abroad. Uncovering the fundamental behaviour of URM constituents and assemblies is essential to inform rational assessments, feasible rehabilitations and alterations in professional practice, including structural and/or seismic upgrading. Damaging earthquakes experienced in moderate seismic zones of Eastern Canada can cause significant losses to the existing building stock [12,13], particularly to URM structures, highly vulnerable to even relatively low-magnitude events [14,15]. Data from uniaxial compression and shear-compression tests are especially relevant in the context of both expeditious evaluation checks (e.g. analytical in-plane (IP) and out-of-plane (OOP) load capacity of URM walls – see [16]) and numerical modelling-powered structural analysis [17,18]. A solid foundation of experimentally derived URM parameters is needed in Canada, yet now still missing. Nevertheless, the authors acknowledge previous pioneering experimental studies in Canada that have targeted masonry typologies at varying scales, particularly Sorour et al. [19] with lateral load testing of stone URM walls, a part of a campaign to restore the Ottawa West Block of Parliament [20,21]. Other tests were completed on stone or brick URM components under IP diagonal compression or shear-compression loading [22,23]. Notably, each of these was conducted on replicated samples, manufactured in the laboratory using modern materials and admittedly targeting reasonable URM mechanical features aligned with international trends – an unsupported assumption related again to the lack of in-situ data.

Research abroad has shown the advantages of testing URM assemblies/components directly in-situ with either minor destructive or destructive experiments, including flat-jack tests [24,25], IP diagonal compression [26–29] and semi-cyclic loading [30] tests, or via OOP airbag testing [31]. This is still a largely unexplored avenue in Canada, where the limited timeframe between cold seasons often makes complex in-situ studies logistically challenging. While the use of non-destructive testing (e.g. ultrasonic pulse velocity – see e.g. [32] and [33]) has proven effective in estimating critical properties of large URM datasets regionally [34–36], the essential correlation with destructive test data [37–40] is still unavailable in Canada. Generally, gathering materials in-situ to be tested later in the laboratory is seldom possible due to site constraints, heritage regulations or required specialized equipment, while extraction may yield specimens that do not conform to available testing standards. In Canada, mechanical laboratory tests on extracted URM constituents are limited to those of [41] on old mortars and [42] on vintage clay bricks. Those on URM components are confined instead to the recent studies of Davis and Malomo [42], who applied diagonal compression on multiple full-scale 19th century two-wythe URM walls with an attached veneer and timber inclusions, and to those on single-wythe URM walls with a timber backup by Paquette et al. [43]. In the US, Atkinson et al. [44] completed shear-compression tests using a direct shear apparatus with shear box specimen holders for one bed joint of running bond samples on three field-extracted URM samples in addition to 51 laboratory constructed replicated samples in a parametric analysis to investigate old/new clay units, cement-lime mortar ratios and joint thickness. Beyond North America, similar attempts at the assembly scale have only been made by Dizhur and Ingham [6] for tests of extracted masonry walls under diagonal compression in New Zealand. At the component-scale, extracted masonry triplets were tested in compression [8,45] and shear [8] in New Zealand and uniaxial compression tests on extracted samples in Turkey by Ispir and Ilki [46] and Ucer et al. [47]. Researchers have also focused on retrieving in-situ small URM samples to be evaluated in the laboratory, through tests of cylindrical cores able to be evaluated for compression and/or shear behaviour as completed in Italy [39,48–50], Spain [1,38,51–53], The Netherlands [54–56] and Australia [57]. Wet coring, as discussed in Cabané et al. [40], is extremely challenging when dealing with lime-based mortars due to their tendency to liquefy. Dry coring [52] solves such an issue but inherently creates vibrations, possibly disintegrating joints when adhesive bonds are weak – this is an issue we have indeed faced in this work where in-situ mortars have endured local harsh climate conditions. Regarding individual URM constituents, namely units and mortars, local experimental data remains largely unrepresented in literature; thus, code provisions rely on parameters often from internationally sourced materials.

This study is the first in Canada to quantify experimentally the uniaxial compression or shear-compression responses of URM constituents and assemblies extracted from local old buildings typical of Eastern provinces. It proposes an alternative method for the extraction and mechanical characterization of old URM assemblies in controlled conditions, targeting three brick-tall prisms (hereinafter referred to as *triplets*). These procedures, as further discussed below, leave more regular and easier-to-repair openings, as well as specimens visually in better physical conditions, while also providing – as cylinders – the possibility of quantifying *both* uniaxial compression and shear-compression (simply named as *shear* in the rest of the paper) complying with widely adopted testing standards. Overall, 59 URM samples were retrieved from four existing buildings in the Greater Montréal (QC) area, erected between 1880 and 1913 for four distinct original end uses. With respect to previous international research, our campaign presents relevant novelties on multiple fronts, as the first cyclic compression tests of field extracted masonry in addition to the first combined elastic and plastic analysis for compression and shear behaviour of field extracted masonry.

Results obtained provide foundational experimental data, previously missing in Canada, on the fundamental mechanics of local URM when subjected to uniaxial compression or shear actions at the constituent and assembly scales. The relevance of the collected URM inventories lies in the unprecedented identification of reference mechanical values and their range of variation among different masonry types and structures built with traditional materials and construction techniques adapted to the Canadian context, in distinct eras. While the authors do recognize that the outcomes presented herein are not conclusive given the intrinsically limited sample size coupled with inherent URM variability, this study represents a first step towards closing the gap with respect to other earthquake-prone countries which have – after decades of research – compiled comprehensive inventories of reference URM mechanical properties in support of their building codes and design guidelines.

2. Compressive and shear behaviour of unreinforced masonry

The nature of the mechanics related to URM behaviour under compressive or shear actions can be described by the complex interaction between its constituent materials, characterized by heterogeneous, anisotropic and nonlinear behaviour [58]. The individual mechanical properties of the units and mortar also influence the overall composite response at the assembly scale, affected as well by workmanship and environmental factors including bond pattern, material and construction quality, exposure to salts, frost damage and alterations (e.g. maintenance, additional construction/renovation phases) [59]. Considering these aspects, experimental studies (mostly on replicated samples) have demonstrated that the stress-strain relationship of masonry under uniaxial compression is governed by two main phases: a linear elastic relationship until cracking followed by progressive fracturing and stiffness/strength reduction (or degradation if considering cyclic loads) in a nonlinear post-peak softening response [60,61]. Experimental tests are typically completed on masonry prisms or wallets, including tests completed on unreinforced and reinforced specimens to investigate strengthening measures e.g. Vintzileou, Miltiadou-Fezans [62]. Failure mode and overall masonry compressive capacity are largely dependent on the relative strengths of units and mortar, where mortar resistance directly affects assembly strength and stiffness [63–65]. Extensive experimental campaigns have been completed to characterize various types of masonry in compression including those with units made of stone [34,66–69], concrete [70–74], brick [75–80] and other materials, namely earthen masonry [81–83] and earthen mortar masonry [84,85].

Similarly, various combinations of unit types coupled with different mortars have been investigated experimentally under uniaxial compression such as work by McNary and Abrams [86] testing clay brick masonry with four mortar mixes varying cement:lime:sand ratios, Soleymani et al. [87] for clay brick units with gypsum mortar or three different lime mortar mixes, or Liang et al. [88] testing clay brick units with mud, lime, cement-lime or cement mortar mixes. The authors refer interested readers to state-of-the-art reviews for further examination on the compressive behaviour of diverse masonry types e.g. Salmanpour et al., [37,89]. Several empirically developed predictive equations are available in codes and guidelines internationally to determine masonry strength from unit and mortar strength including Eurocode 6 (Eq. 1), where f_b is the brick compressive strength, f_j is the joint compressive strength, and K, α and β are constants given the type of masonry and configuration. Similarly, the Australian standard AS3700 (Eq. 2) relates unit strength to the geometry and relative mortar strength (k_m is a mortar strength factor and k_h is the unit-to-mortar joint thickness ratio). These predictive equations have been calibrated on masonry types not typical of Eastern Canada, requiring proper validation, as done abroad by e.g. Kaushik et al. [61].

$$f'_m = K f_b^{\alpha} \times f_j^{\beta} \tag{1}$$

$$f'_m = k_h k_m \sqrt{f_b} \tag{2}$$

Section 7 of this work further investigates the applicability to the Eastern Canadian field-extracted masonry tested herein. Canada's CSA82 utilizes tabulated values based on unit and mortar type to estimate masonry compressive strength of modern, intact assemblies – not applicable to existing URM.

URM lateral response at the (isolated) global component level (e.g. wall) is typically associated to multiple different failure modes related to assembly-scale shear-axial coupled mechanisms, either governed by adhesive/frictional (bed-joint sliding) or tensile (head-joint cracking, diagonal tension failure through the joints or units) stresses [90]. These are dependent on the interaction across scales between geometry, boundary conditions and material properties of URM constituents, assemblies (whose properties are indeed embedded into capacity formulae for URM members) and the whole component, providing global indicators of IP structural performance. Experimental tests used to quantify the shear strength of URM assemblies include small-scale tests as direct shear tests (EN 1052) on masonry triplets/couplets [44,76], or mid-to-large tests on components tested in diagonal compression (see e.g. [91] or [92], via ASTM E519 or RILEM LUM B6 and its variations) or under IP shear-compression [2,93,94]. For characterizing existing masonry in shear, in-situ minor destructive tests and destructive tests include the shove test (ASTM C1531) [95], often combined with the used of flat jacks to apply desired axial stressors [96], shear tests on cores [50,53,55] and in-situ diagonal compression tests [6,29]. Research from the past decades has established that the Mohr-Coulomb criterion (Eq. 3) adequately describes joint shear behaviour at low levels of precompression stresses (i.e. when unit does not crush). Eurocode 6 (EN1996–1–1, Eq. 4), Canada's CSA S304 (Eq. 5, only applicable in principle to the design of new structures), US' TMS 402/405 and the New Zealand [97] code (these last two use Eqs. 6c, 7) all prescribe equations for shear strength based on the Mohr-Coulomb form where σ is precompression axial stress, τ_u is the ultimate shear strength, c is cohesion, and φ is the friction angle. For consistency with the source documents, notations and definitions of variables used in herein are retained as presented in the respective codes and standards from which the equations are derived. These definitions apply only within this section and will be redefined as necessary in the remainder of the paper. In Eq. 6, V_{nm} is the nominal shear strength of an unreinforced shear wall in strength design for non-grouted solid running bond masonry where f'_m is the masonry compressive strength, A_{nv} is the nominal area and N is the axial force. It should also be noted that in TMS 402–22 the strength reduction factor for shear is 0.80 and considers imperial units. For Eq. 7, V_{sl} is the shear sliding capacity, where t_{nom} is nominal thickness, L_W is the component length, μ_f represents the masonry friction coefficient, P is the superimposed deadload at the top of wall/pier and P_W is the self weight. It is important to note that Eqs. 3, 4, and 5 define the local shear properties of masonry assemblies, while Eqs. 6 and 7 apply to masonry components for global behaviour definition.

$$\tau_u = c + \sigma \tan \varphi \tag{3}$$

$$f_{vk} = f_{vk0} + \mu_k \, \sigma_d \tag{4}$$

$$v_m = v_{m0} + 0.5 \quad \sigma_v \tag{5}$$

$$V_{nm} = min : \{(a)3.8\sqrt{f'_m}A_{nv}, \ \ (b)300A_{nv}, \ \ (c)56A_{nv} + 0.45N\} \tag{6}$$

$$V_{sl} = 0.7[t_{nom}L_W c + \mu_f(P + P_W)] \tag{7}$$

Eurocode 6 (Eq. 4) adopts a structure where the characteristic shear strength (f_{vk}) is calculated using the characteristic initial shear strength at zero stress (f_{vk0}), determined from tabulated values based on extensive testing previously done for different materials, and the design compressive stress perpendicular to the shear plane (σ_d) and a friction coefficient (μ_k) of 0.6 for joint shear strength. It should also be noted that the characteristic value of the shear strength (f_{vk}) as used in Eurocode 6 is taken as 80% of the experimentally measured values. CSA S304 (Eq. 5) uses the Mohr-Coulomb form as well to calculate shear strength (v_m) based on the experimental base shear strength (v_{m0}), coefficient of friction of 0.5 and the vertical compressive stress (σ_v). The equations above are all based on the same mechanics yet their form – with the exception of Canada – is tailored to the respective regional contexts.

3. Unreinforced brick masonry in Eastern Canada

Brick URM is predominant in Eastern Canada, used in up to 70% of the regional building stock in densely populated old urban centres and present in most envelope and non-structural components in both traditional and modern low-to-mid-rise constructions [98]. This is intimately tied to Canada's history, whose critical and targeted review is essential to understand the rationale behind local construction practices and the employment of specific materials and techniques. This section briefly summarizes these aspects to provide essential background to readers, otherwise referred to [99,100] for more details. Critical details are also given on the various buildings from which the URM samples tested within this experimental campaign were retrieved, alongside their main features.

With the exponential growth of organized communities along the St. Lawrence River, as the national focal point of industry, trading and commerce in the 19th and 20th centuries, came expansive urbanization across all sectors [101–103]. At the same time, damage from fires (e.g. 1845 Québec City, 1852 Montréal) spurred lawmakers to ban the construction of entirely timber buildings in city centres in favour of stone or more frequently brick masonry bearing wall constructions [104], made cheaper with mechanized brick production in the 1850s [105,106]. Construction of URM buildings in these times followed traditional building practices and architectural preferences influenced by international trends and earlier European colonization, resulting in unique adaptations to fit available local materials and technologies amidst harsh environments [107,108]. URM structures from the 19th to early 20th centuries are indeed constructed with timber interior diaphragms, adopting "slow burning" mill style framing systems characterized by heavy-timber beams and columns paired with thick floors (min. 10 cm or 4") without joists to limit the spread of fires [109]. Despite their prevalence, experimental studies into the structural behaviour of these vernacular systems in Eastern Canada are limited to shake-table tests of brick masonry veneers attached to wood board backups [43] and

diagonal compression tests of extracted masonry walls with timber inclusions [42]. Results from characterization tests on original URM samples under compression or shear are missing altogether, with local practitioners wrongly referring to older manuals mostly from the US (e.g. [110]) reporting reference values obtained sometimes a century ago with unclear procedures or controls.

In this work, four URM archetype buildings located in Montréal, yet representative of Eastern Canada's older construction forms and encompassing as many original uses (residential, critical infrastructure, industrial, institutional), were chosen as case-studies supported by comprehensive archival and engineering history studies [99,111]. In Fig. 1, these buildings are identified using location-based acronyms.

The first building is a 1910 residential structure (BBE/BBL), erected in the Queen Anne revival style with a mansard roof. This building is typical of the multi-family residences constructed across Eastern provinces [103], featuring two-wythe loadbearing masonry transversal party walls and veneer façades weakly coupled to a light timber framing backup. The loadbearing walls contain weaker, lighter coloured solid clay bricks with lime mortar (BBE), while veneers have better quality facing units coupled with an analogous yet black-pigmented mortar (BBL). This building also notably contains horizontal timber inclusions throughout the wall height on the interior, for finishing purposes. BSC is a 1892 fire station, now housing a municipal library, characterized by mass masonry return walls, a stone front façade, timber interior framing and a stone foundation [112]. STP is a 1913 industrial building located along the Lachine canal, characterized by mass masonry walls and a heavy timber internal framing system typical of the "slow burn" mill construction. The final building (VAN) is a 1904 originally designed for hosting various critical services (city hall, fire station, post office and police station) a public library [113]. VAN has loadbearing masonry walls with embedded steel frames, mostly likely constructed in a cage-frame system [111,114]. Table 1 summarizes the building type, location and materials extracted for testing in this work.

Table 1
Summary of key features of the URM archetypes from which the samples tested in this work were extracted.

Building site	Built date	Montréal area	Building details	Brick type	Materials extracted
BBE/BBL	1910[a]	Plateau	Three-storey residential building	Solid	Bricks, mortar, triplets
BSC	1892	Le Sud-Ouest	Three-storey old fire station	Frogged	Bricks, mortar, triplets
STP	1913	Pointe-Saint-Charles	Two-storey industrial building	Frogged	Bricks, mortar, triplets
VAN	1904	Petite-Bourgogne	Three-storey critical infrastructure	Solid	Bricks, mortar, triplets

[a] Estimated construction date provided by Hardy Inc., the renovation specialists in charge at the time samples were retrieved onsite

4. Mechanical characterization of old masonry constituents

The procedure for the URM sample extraction, developed and employed herein for the specific masonry type and pattern (adapted American common bond – header every 4–5 courses) encountered in the selected building archetypes is defined in this section along with the mechanical characterization of unit and mortar constituents.

4.1. Masonry field-extraction procedure

Despite the successful application abroad of URM coring as a mean to seamlessly extract intact samples, as discussed earlier, this technique in its various declinations (wet, dry) was found ineffective in our study. When used onsite, coring always yielded fractured samples due to distinct yet explainable reasons. In Canada, climate stressors coupled with less refined workmanship and production methods often reduce bond adhesion to minimum values – as confirmed by the experimental results presented later in this paper. The bond would simply not withstand the dry coring vibrations. When water was added also to mitigate the diamond coring bit overheating (increased by the rough texture of local old clay bricks, often featuring rock clusters and other solid inclusions), the mortar would liquefy due to the soluble lime solution in mortars. Further, the bond pattern used here limits the areas from which single-wythe samples can be extracted (must be in the running bond regions, among the horizontal header lines used as ties) which makes it impractical to use a portable rig-mounted coring machine in older occupied buildings. Extracting prismatic samples instead – namely triplets – has proved ideal in this work and yielded visually intact specimens with relatively low effort. The additional advantage of retrieving triplets as opposed to cored cylinders or wallettes is the fact that reference North American standards accepted here for compression – ASTM C1314 (US) in particular as its Canadian counterpart is not available – deem such geometry as compliant using correction factors. Similarly, EN 1052–3 allows triplets to be tested in shear under increasing precompression. The extraction of URM samples used herein is also context-adapted.

Canadian old mortars are particularly friable, and bonds are weak in relation to clay bricks. Joints are also often thicker than 10 mm, which allows cutting through them without touching units. Making parallel vertical incisions in the URM to separate samples inevitably entails passing through some bricks. However, doing it every other brick allows vibrations to disperse and avoids early damage to horizontal joints leveraging existing axial compression loading path within the building. After cutting the top horizontal joints intercepting previous vertical incisions, sample extraction can be completed by using a lever inserted into a hole drilled in the middle of the mortar joint while imposing axial compression manually, so that triplets shear off the wall. This is enabled by the fact that the running bond areas among header lines are only



Fig. 1. URM archetypes from which samples tested in this work were extracted, with location-based acronyms.

attached vertically through mortar binding. Finally, extracted samples were wrapped using adhesive tape, placed in insulated containers with foam/paper and transported to the laboratory. The use of the *Berrouard Method* (in honour of the remarkable City of Montréal's in-situ coordinator supporting our research), allowed us to retrieve old masonry constituents (161 mortar chips, 71 bricks) and assemblies (28 triplets) from the external walls using general-use power tools, minimizing post-extraction repair works. The process is depicted in Fig. 2, in six main steps.

All extracted specimens presented some degree of geometrical irregularity, due to both the extraction procedure and the morphology of the masonry constituents (joints of varying thickness, bricks protruding horizontally, warping and uneven brick surfaces). The potential implications of these irregularities could not be quantified experimentally, albeit the authors reasonably believe these to be of limited influence on the measured mechanical responses. Such irregularities were indeed outside of the main load path, representing localized deviations from idealized geometries that would hardly affect global assembly-scale mechanics.

4.2. Physical and mechanical properties of old bricks and mortars

This sub-section presents the experimental methods and results used to determine the mechanical features and responses of the field-extracted materials under the selected laboratory protocols. Physical properties are summarized in Table 2 where the geometries, density and type of bricks are also included. Chemical properties were also inferred for the older lime based mortars – comprising minor proportions of Portland cement added to sand, calcium oxide, soluble silica, and magnesium oxide – and presented in a separate article of potential interest to readers [41].

Individual half bricks from each building site were tested in the laboratory to determine compressive strength and elastic properties according to ASTM C67. Uniaxial compression tests were performed under displacement control at a constant rate of 0.0085 mm/s in a 4500 kN MTS load frame. Vertical strains were measured using two 50 mm extensometers attached to the vertical brick face, as shown in Fig. 3a,b. Brick beds were capped to 25 mm thick steel plates using a high strength gypsum compound [115]. Results are summarized in Table 3, including the coefficient of variations (COV) for compressive strength (f_b) and Young's modulus (E_b). Outliers were detected using the interquartile range (IQR) method and 1/70 values for compressive strength and 4/70 values for Young's Modulus were determined as such. The single outlier for compressive strength in VAN was characterized by a significantly darker color than other samples, potentially contributing to strength increase based on clay firing conditions e.g. proximity to furnace and heat, inherent to the manufacturing process [116].

Mortar strengths were derived from joint fragments (or *chips*) extracted from head and bed joints surrounding the extracted masonry samples using the double punch test (DPT). DPT applies uniaxial compression (or "punching") with increasing monotonic displacement of 0.1 mm/min to samples through 20 mm diameter steel punches at the top and base of the chips. Specimens were sanded to prepare an even surface and then capped with a high strength gypsum mortar in a uniform thickness and diameter (1 mm×30 mm) to prevent premature failure and underestimation of strength. This procedure is adapted from the DIN-9022 standard [117], used by researchers specially for cases when prismatic mortar cubes cannot to be obtained [40], as is the case in the majority of existing buildings. Mortar (cubic) compressive strength (f_j) is back-calculated from the maximum DPT force between steel punches and adjusted according to Eq. 8 [118] considering sample thickness (t) and friction at the steel punch/mortar interface (μ).

$$f'_j = n(1-\mu\eta) \times \frac{\beta^2(1+k_t)+(1-k_t)}{\beta^2(2+k_t)-k_t} \tag{8}$$

In Eq. 8, $\beta = R_e/R_i$ relates the inner radius of the steel punch (R_i) to the radius of the circle of the mortar specimen (R_e), $\eta = R_e/2t$, and k_t is the ratio between mortar tensile and compressive strength, adopted as 0.1 as recommended by Benedetti and Tarozzi [118]. Resulting compressives strength values using this equation are comparable to standard cube compression tests, with the closest agreement for DPT tests on specimens with a thickness of 20 mm [41]. Mortar cubic compressive strength values from DPT using Eq. 8 are presented in Table 3 and considered in the rest of this article for joint strength. Failure involves radial cracks spreading from the edge of the loading punch, as shown in Fig. 3d.

The inverse relationship between DPT mortar compressive strength and sample thickness can be represented by a power law, where the specimens with the minimum thickness show a higher stress and a higher thickness display lower stress, as confirmed by previous studies [41,118,119] and also seen in Fig. 4. In the latter, the applied axial stress of each sample is plotted against the sample thickness and the mean f_j ($\overline{x}$, red) and ±1 standard deviation ($\overline{x} \pm s$, blue) of each building are superimposed. The high strength values skewed to low thicknesses (5–10 mm) can be attributed to the higher confinement and boundary condition effects or material heterogeneity, which show less dispersion at greater thicknesses [41]. In the case of BSC, specimens thinner than 8 mm exhibited artificially elevated strengths, thus averages were calculated from specimens between 8 and 19 mm to represent in-situ mortar joint thickness and prevent an overestimation of the mortar compressive strength. An average compressive strength across the sites of 2.34 MPa shows good agreement with strength values from Type-O mortar, a commercially available mortar mix often recommended for old URM containing a 1:2:9 ratio of cement:lime:sand by volume, measured in a prior experimental campaign using cube compression tests of 50x50x50 mm^3 samples (2.4 MPa) [42].

Brick compressive strength and Young's moduli values display the variability inherent in existing buildings and the need to test local materials. BSC and STP, despite the same brick type and color, vary in strength by 250%. Indeed, within the same structure BBE/BBL behave differently, where the interior structural bricks (BBE) are less than half

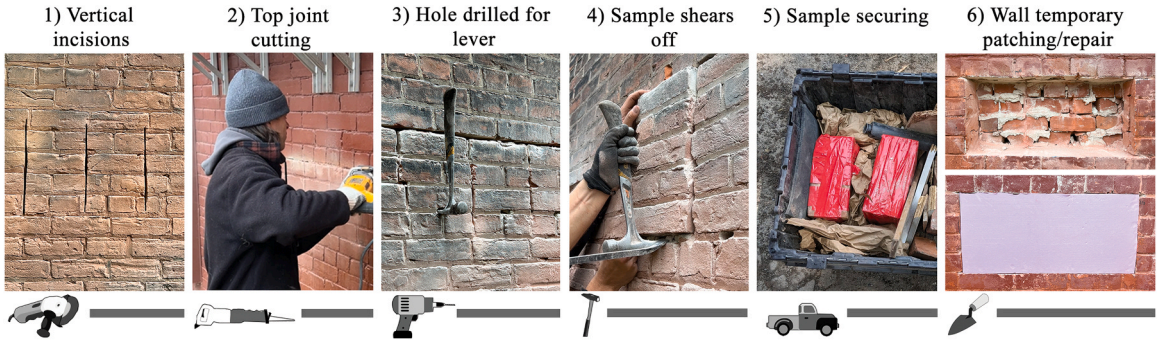

Fig. 2. Employed URM assembly field-extraction procedure (*Berrouard Method*) based on six main sequential steps.

Table 2
Main physical properties of masonry constituents and assemblies.

Specimen type	Brick type	Brick size (mm^3)	Brick density (kg/m^3)	Joint thickness (mm)	Mortar density (kg/m^3)	Prism dimensions (mm^3)
BBE	Solid	205x93x61	1797	12.0	0.0026	138x94x178
BBL	Solid	204x97x62	1845	9.0	0.0019	169x89x202
BSC	Frogged	202x97x65	1484	11.0	0.0015	202x95x209
STP	Frogged	197x93x60.5	1796	11.0	0.0019	197x93x207
VAN	Solid	207x92x63	1770	11.0	0.0018	207x92x210

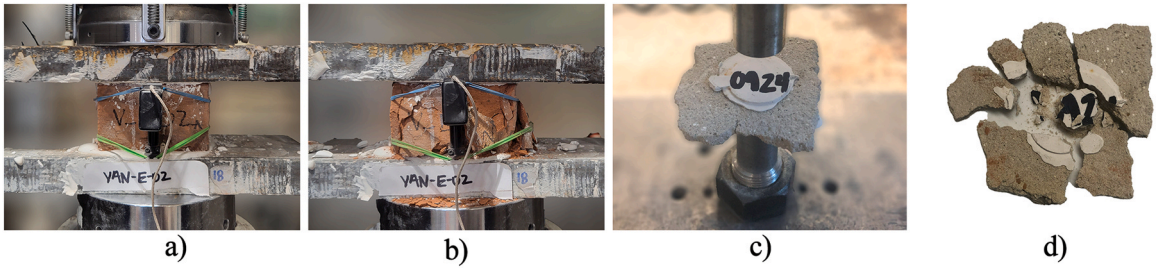

Fig. 3. a) Uniaxial brick compressive strength mechanical test setup and b) failure mode; mortar double punch test c) mechanical test setup and d) failure pattern.

Table 3
Mechanical characterization results of masonry constituents based on a sample size *n*.

Building site	Brick type	Colour	*n*	f_b (MPa)	COV (%)	E_b (MPa)	COV (%)	E_b / f_b	*n*	f_j (MPa)	COV(%)
BBE	Solid	Orange	20	11.5	40	1665	44	317	31	2.69	73
BBL	Solid	Red	20	26.9	17	3804	39	284	42	2.03	60
BSC	Frogged	Red	12	17.3	14	832	30	141	23	2.25	77
STP	Frogged	Red	10	60.6	31	19871[a]	40	170	27	2.11	58
VAN	Solid	Red	9	28.3	21	8174[a]	36	353	38	2.40	65
Average				28.9	25	6869	38	253		2.34	66

[a] Young's modulus calculated from only 5 of the *n* specimens tested due to equipment reading error

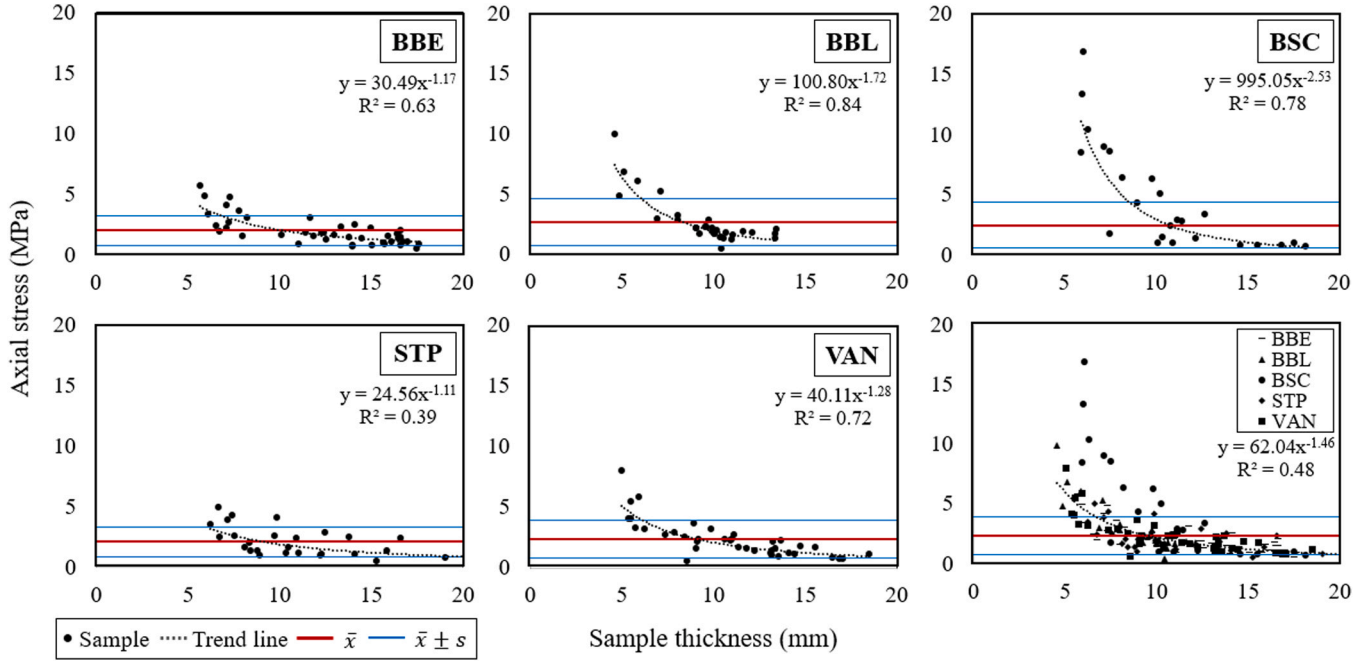

Fig. 4. Double punch test results: sample thickness vs applied axial stress.

the strength of the exterior face bricks (BBL). This difference can be attributed to the exposure of face bricks to weather conditions, purposely manufactured with lower porosity values which often results in higher brick compressive strengths from the vitrification process [7, 116]. COV values for brick compressive strength were lower than for stiffness measurements, 25% vs 38% on average, as seen in similar tests

of existing clay brick samples [7] and similar levels of variance were noticed by other researchers [45]. Results in Table 3 seem to agree well with previous studies e.g. Lumantarna et al., [30,45,54]. Comparing brick unit strength to unit modulus of elasticity, the E_b/f_b relationship can be described by $E_b = 244 * f_b$ (R^2=0.81). These correlations become essential for preliminary studies and verifications when limited data or access to sites are limited, as it is often the case in Eastern Canada.

Bond wrench tests according to ASTM C1072 were also completed for each masonry type to evaluate strength at the unit/mortar interfaces. Results from bond wrench tests display limited strength at the unit-mortar bond, as failure occurred below a measurable point (<5.6 Nm). Bricks were easily lifted from mortar bed by hand. The minimal interface bond can be explained by the age of the samples and the materials [120], where adhesive strength in the form of cohesion is further investigated using triplet shear tests in Section 6.

5. Uniaxial compression testing of old masonry assemblies

41 extracted masonry triplet specimens were tested under uniaxial compression in displacement control following the ASTM C1314 standard's detailed specifications for field-extracted samples. The latter were prepared following ASTM C1587/C1787M to the best of the authors' abilities, following the practical guidance provided for the preparation of existing URM specimens. No additional preparation was required for the samples in this work beyond the removal of excess mortar on the loading surfaces and the leveling and capping of the triplets to 25–40 mm thick steel plates using a high strength gypsum cured for at least 24 h. Monotonic tests were performed on a 4500 kN MTS load frame at a constantly increasing displacement of 0.01 mm/s where axial displacements were measured with two vertical linear vertical displacement transducers (LVDT, displacement range ±15 mm) glued to the steel bearing plates and two horizontal LVDTs glued to the masonry spanning across the central head joint. Cyclic loading was applied to a subset of the field-extracted samples, where increasing loading and unloading cycles were prescribed at intervals of 0.5 mm in the displacement-controlled procedure, followed by monotonic loading after 5 mm of measured displacement of the actuator. Loading and unloading cycles were completed three times at each prescribed displacement. Tests were stopped after 20% of peak force capacity was reached or when specimen damage was visibly assessed to a point where continuing to test would damage equipment. While cyclic procedures are not codified in available Canadian standards, the procedure applied herein was modeled after prior experimental studies on replicated masonry prisms [121,122].

5.1. Monotonic compression results

Failure progression of masonry triplets in monotonic compression developed with no visible cracking observed before peak force, followed at the force peak by visible vertical cracking, spalling along brick extremities and mortar crushing. Majority of the crushing in bricks was observed within the middle row, similar to Gumaste et al. [79]. Representative undamaged and damaged samples from each building are shown in Fig. 5.

Results from LVDT and actuator data were processed to calculate mean compressive strength (f_m), Young's modulus (E_m) and fracture energy in compression (G_c), presented in Table 4. Fracture energy is calculated as the area under the stress-displacement curve, from zero until ultimate displacement according to the same procedure outlined in [123]. As tests were stopped after around 10–20% of maximum force, ultimate displacement was calculated with linear regression, considering the slope between $0.5\ f_m$ - $0.3\ f_m$ and following the procedure used by Lourenço et al. [124] and Jafari et al. [54]. Horizontal LVDTs spanning the central head joint were implemented to capture longitudinal strain. Poisson's ratio (ν) was taken as the ratio of lateral strain to axial strain between 1/10 and 1/3 of the maximum stress, as done by e.g. Cuadros-Rojas et al., [125]. Based on the deformability of the head joint, calculated values of Poisson's ratio presented unrealistic results (range of $\nu = -0.2 - 1.2$), thus are not further included. These results are potentially explained by the lack of lateral confinement around the head joint as similar research conducted on replicated masonry wallets e.g. Augenti and Parisi [126] and Jafari et al. [123] included additional lateral confinement whereas results from tests on stack bonded prisms record the lateral deformation of only the brick [64,125]. Results presented in Table 4 includes measured strength values and scaled values, which account for the triplet aspect ratios as recommended by ASTM C1314.

The compressive strength values indicate variations (13–59% COV) expected when testing existing materials, as seen in Lumantarna et al. [45] 12–25% COV, and Ispir and Ilki [46] 31% COV. Kaushik et al. [61] also noticed higher strength dispersion in samples with a strong brick to weak mortar combination (24% COV, vs 18–20% COV for prisms with

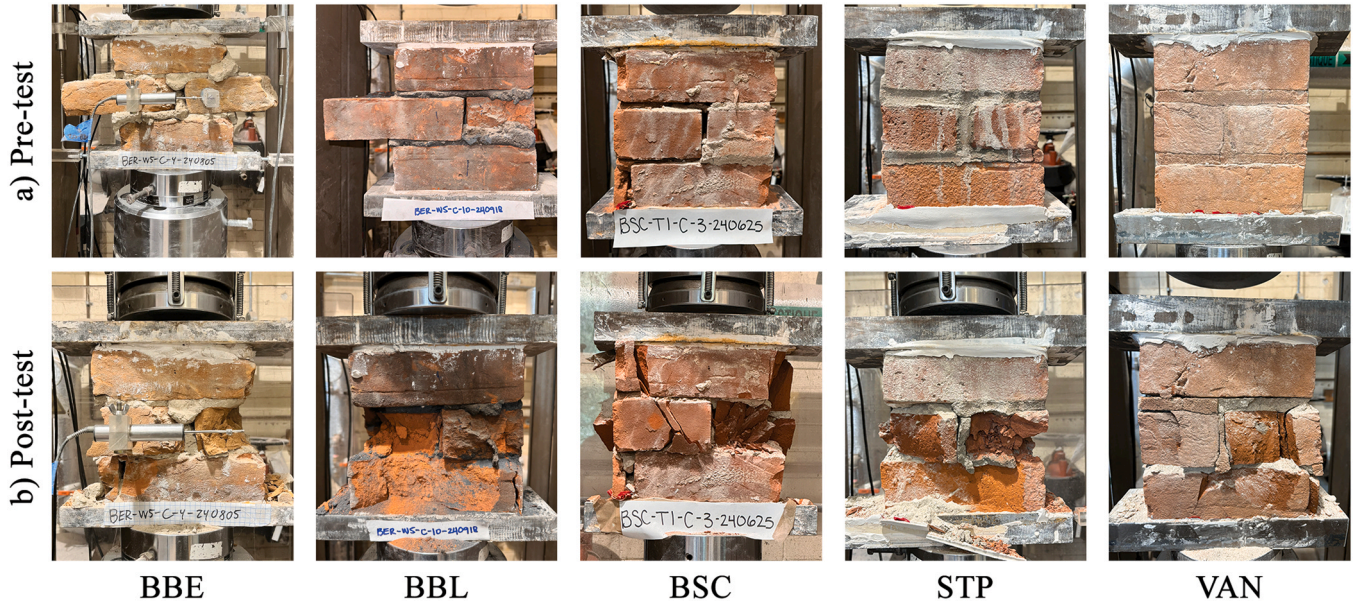

Fig. 5. Monotonic compression tests: a) initial vs b) post-failure conditions of URM specimens.

Table 4
Monotonic compression results for field-extracted URM (triplet) assemblies.

Specimen type	n	f_m (MPa)	COV (%)	f_m (scaled)[a] (MPa)	E_m (MPa)	COV (%)	ε_{peak} (mm/mm)	COV (%)	E_m / f_m	G_c (N/mm)	COV (%)
BBE	7	5.7	32	5.0	762	60	0.019	37	135	17.3	22
BBL	6	14.1	36	12.9	1371	39	0.024	48	97	46.1	51
BSC	3	3.4	13	2.9	1894	22	0.007	11	559	27.3	1
STP	5	7.1	59	6.0	680	52	0.038	85	95	50.3	34
VAN	8	7.4	17	6.3	1081	37	0.016	19	146	48.6	17
Average		7.5	31	6.6	1157	42	0.021	40	206	37.9	25

[a] Correction factors from ASTM C1314, example aspect ratio/correction factors: 1.0/0.83, 1.25/0.93, 1.5/0.96. Linear interpolation for aspect ratios between those listed.

intermediate or strong mortar). In the case of STP with the largest COV (59%), triplets with two distinct brick/joint layout configurations were tested, with either half (HB) or full (FB) bricks in the middle course on either side of the central head joint. Considering the two configurations, HB triplets had an average f_m of 4.3 MPa (40% COV) whereas the FB ones retained f_m of 11.4 MPa (18% COV). The geometrical difference can contribute to the larger variation, yet it is just as likely that the ratio of brick to mortar strength plays a role as STP has the highest f_b/f_j ratio.

Fig. 6 presents axial stress-strain curves for all specimens, capturing peak compressive strength and post-peak softening behavior. Envelope curves bound the specimen curves, revealing variability inherent to field-extracted material with the mean ($\overline{x}$, red) and ±1 standard deviation ($\overline{x} \pm s$, blue) superimposed to characterize the statistical dispersion of strength and stiffness within this heritage masonry dataset. A graph depicting the relationship between f_m and E_m is also included in Fig. 6, where the relationship of $E_m = \alpha f_m$ was determined with linear regression, where $\alpha = 135.3$ and $R^2 = 0.63$ – this is comparable to results from literature, yielding $\alpha = 50$–230 with 0.46–0.68 R^2 [63,64] for replicated clay brick URM with lime mortars.

G_c values found herein (17.3–50.3 N/mm) are within the range previously reported in literature. Jafari & Esposito, [127] showed values between 33.77 and 35.68 (10–15% COV) on monotonic compression tests of replicated clay brick masonry wallets. Tests by Vasconcelos et al. [67] display G_c values of various granites between 11.8 and 49.1 N/mm (3–25% COV) calculated only in the post-peak region.

5.2. Cyclic compression results

Cyclic testing was limited to BSC, STP and VAN specimens whose uniform geometry permitted direct comparison of monotonic and cyclic responses, BBE and BBL were excluded due to dimensional irregularities introduced during their manual extraction. A total of 12 specimens from these three sites were thus subject to cyclic loading. Failure mechanisms of samples were consistent with monotonic counterparts, as the observed damage progressed from vertical cracks in bricks to post-peak spalling concentrated in a cone shaped pattern in the central course

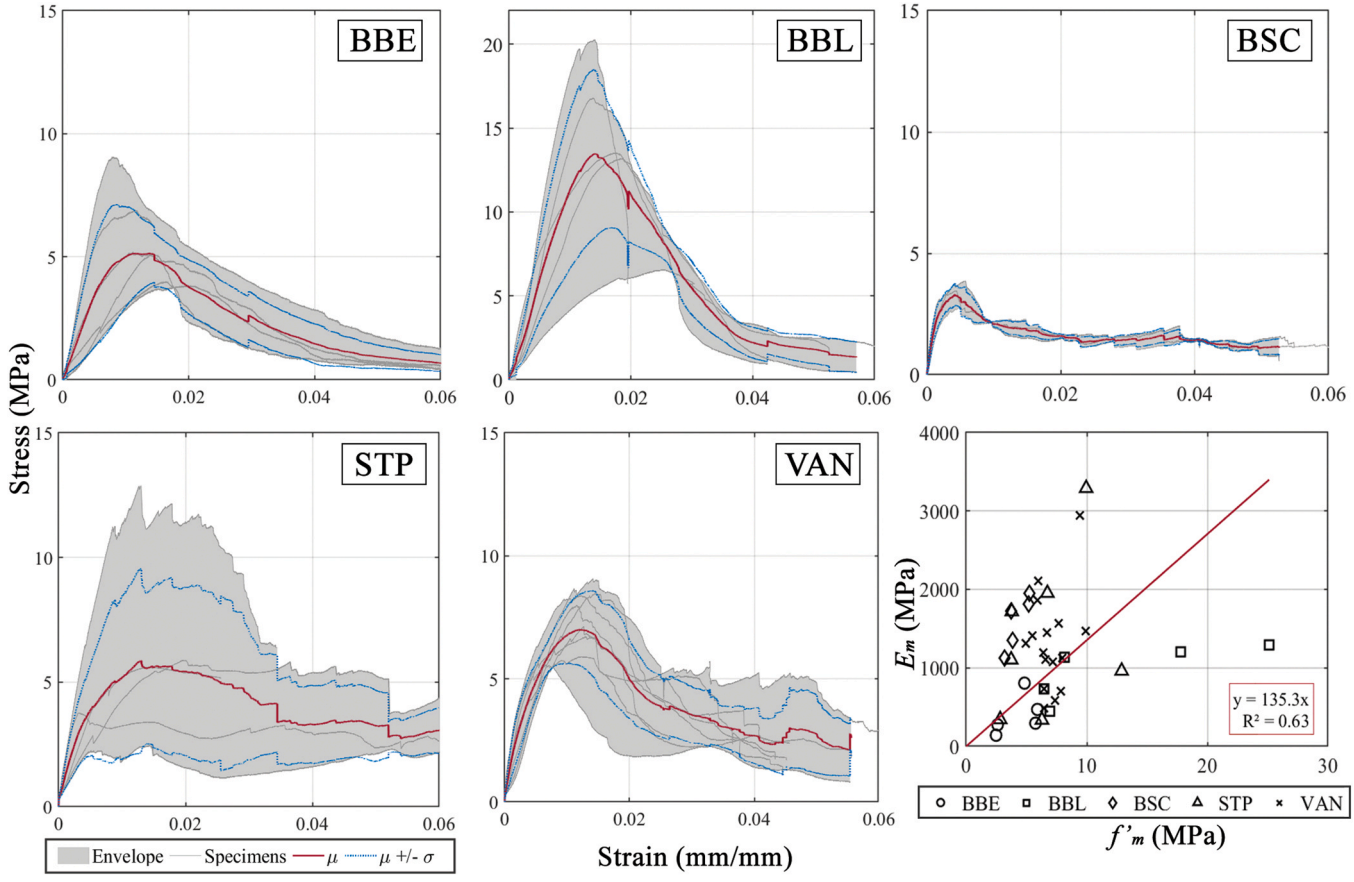

Fig. 6. Monotonic compression tests: stress-strain curves for URM assemblies tested under monotonic compression, and compressive strength and Young's modulus correlation with linear regression plot for all samples (bottom right).



Fig. 7. Cyclic compression tests: damage progression of a URM specimen tested under cyclic compression.

(Fig. 7). Damage at the unit-mortar interface suffered pulverization following crushing in joints and consequent spalling of the exterior portions, seen in Fig. 7 at the bottom of the samples. Concentration of damage occurred primarily at the edges of the samples, similarly to results from cyclic tests of stack bonded masonry prisms by e.g. Ispir, Ilki [46,128]. Vertical cracks through the sides were visible, as seen in tests of running bond prisms by Facconi et al. [129].

Results are summarized in Table 5, where the average f_m, E_m, ratio of Youngs' modulus to compressive strength and G_c are reported. An average compressive strength of 5.9 MPA (21% COV) and Young's modulus of 2.0 GPa (20% COV) for the 12 samples tested was measured. This study, as seen in previous tests [46] on replicated URM samples, show a lower data skew when cyclic loading is used, as opposed to monotonic increments. G_c values reported by Segura et al. [121] for stack-bonded clay brick masonry prisms (5 courses) tested in cyclic compression average 9.75 N/mm (mean compressive strength was 7.10 MPa). The compression fracture energy G_c calculated herein is higher, with an average of 57.3 N/mm for 16% weaker masonry in uniaxial compression, due to the higher ultimate displacement values experienced.

The axial stress-strain backbone curves in Fig. 8 demonstrate a softening phase after the peak load is reached. A few samples experienced a plateau after a certain level of softening, leading to high displacements to unload to 10–20% of the maximum resistance. In the case of VAN, the samples tended to fail at different strain levels. Regarding the cyclic nature of the recorded responses, it is worth noting that prior to the peak stress, on average the measured Young's modulus in the reloading branch was 61% higher than that measured between 10% and 33% of the peak load. This pre-peak stiffening phenomenon was also reported in similar work by [130,131].

With respect to the strain at peak stress in cyclic tests, the ε_{peak} average for all samples is 0.019 mm/mm (41% COV), 10% difference to the monotonic value of 0.021 mm/mm (40% COV). Lower Young's moduli were measured when applying monotonic loads – on average 55% of the value calculated from the cyclic envelope curves (25% COV, Table 6). A higher Young's modulus under cyclic loading than monotonic could possibly be attributed to crack closure and compaction, where early repeated cycles progressively close pre-existing micro-cracks in the material. This phenomenon is observed in rocks under cyclic loading, where the friction between the crack surfaces stops the re-opening of micro-cracks, leading to higher Young's moduli measurements [132]. Similarly, uniaxial compression fatigue tests on rocks also displayed a higher Young's modulus when compared to their monotonic counterparts, explained by the authors as the macro-scale effect of the closing of natural micro cracks and voids [133]. The trends above are not reported for stone masonry, where monotonic and cyclic Young's moduli remain comparable [130]. For replicated (intact) brick masonry wallettes, the Young's modulus from monotonic testing is usually similar or higher when monotonic compressive loads are applied uniaxially [134]. In this connection, Segura et al. [121] found ε_{peak} to be 14.8% lower in cyclic compression compared to monotonic test on stacked brick masonry prisms, yet only a 4% difference in Young's moduli between the two test procedures was observed. Previous tests on extracted brick masonry wallettes show a 5% increase in compressive strength and 6.7% decrease in Young's modulus between monotonic and cyclic specimens, respectively [46]. Of further interest is the reduction in COV of Young's modulus from 42% under monotonic loads to 13% under cyclic loading [46], consistent with the trend observed in this work of 42–20%. Another possible explanation for the trends observed may reside in the relatively low sample size and high variability observed for the Young's modulus throughout this testing campaign.

6. Shear testing of old masonry assemblies

Direct shear (or simply *triplet* hereinafter) tests were completed on the same URM types of field-extracted clay brick presented in the previous sections, according to EN 1052–3. 18 samples from three buildings – BSC, STP, VAN – were tested in shear. As all samples were field extracted with a running bond pattern, tested samples include two brick configurations based on the location of head joints between two half bricks. 10 samples were tested with a whole brick in the exterior courses and half bricks in the central course (T1), as seen in Fig. 9b/c, and 8 samples include a whole brick in the central course and half bricks in the exterior courses (T2), as seen in Fig. 9d. The experimental setup and results for triplet tests are presented in this section.

6.1. Experimental shear testing procedure

Triplet shear tests were conducted with three precompression loads of 0.2, 0.6 or 1.0 MPa applied perpendicularly to the bed joints. Vertical (shear) loads were applied at the top of the centre brick with a monotonically increasing displacement of 0.1 mm/min, in a 150 kN capacity

Table 5
Cyclic compression results for field-extracted URM (triplet) assemblies.

Specimen type	n	f_m (MPa)	COV (%)	f_m,(scaled)[a] (MPa)	E_m (MPa)	COV (%)	ε_{peak} (mm/mm)	COV (%)	E_m / f_m	G_c (N/mm)	COV (%)
BSC	2	5.3	2	4.5	2740	6	0.005	3	514	47.2	29
STP	2	5.3	40	4.5	1835	9	0.057	85	349	65.2	4
VAN	8	7.2	21	6.1	1562	46	0.013	37	217	57.4	15
Average		5.9	21	5.0	2046	20	0.019	41	360	57.3	22

[a] Correction factors from ASTM C1314, example aspect ratio/correction factors: 1.0/0.83, 1.25/0.93, 1.5/0.96. Linear interpolation for aspect ratios between those listed.

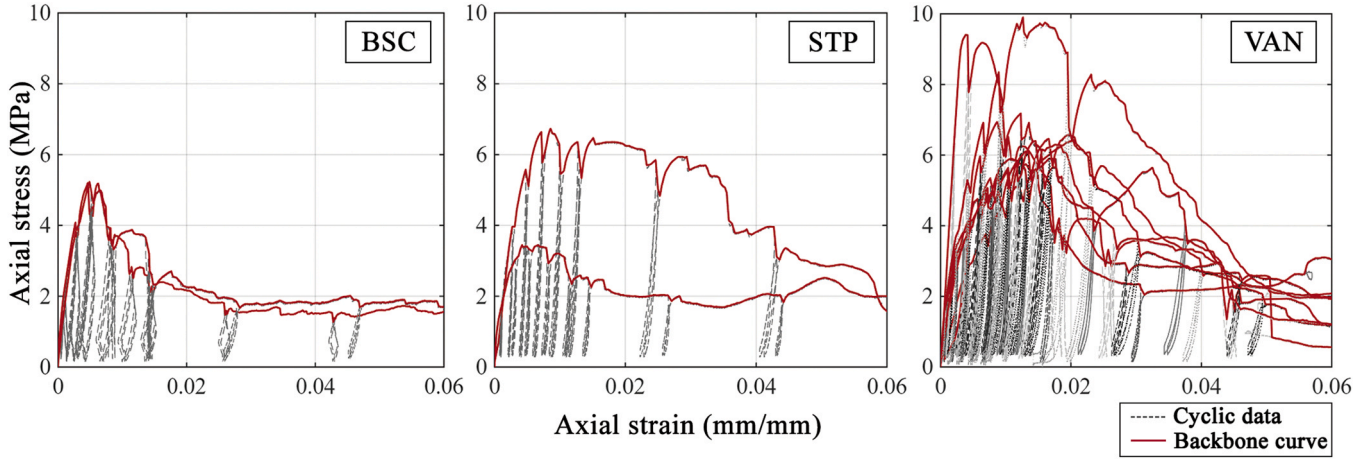

Fig. 8. Cyclic compression tests: stress-strain curves for triplet samples from each building tested in cyclic compression.

Table 6
Monotonic and cyclic compression results summary for field-extracted URM (triplet) assemblies.

Specimen type	*n*	f_m (MPa) (average all samples)	f_m *monotonic/ cyclic*	E_m (MPa) (average all samples)	E_m *monotonic/ cyclic*
BBE	7	5.7	-	762	-
BBL	6	14.1	-	1371	-
BSC	5	4.2	0.64	1917	0.69
STP	7	5.9	1.34	1377	0.37
VAN	16	7.3	1.03	1634	0.69
Average		7.2	1.00	1491	0.57

universal MTS machine, through two 12.7 mm diameter steel cylinders between two steel plates (90 mm x 72 mm x 18 mm in length/width/height), equal to the cross-sectional area of the brick length. At the triplet base, a steel cylinder inserted between two steel plates was placed under the lateral bricks of the specimen, according to the EN 1052 specifications. Specimens were levelled at all loading surfaces and capped to 25 mm thick steel plates at each end with high-strength gypsum (HydroStone 34.5 MPa cube compressive strength, 13% COV) cured for a minimum of 24 h. Each specimen was fitted with four LVDTs (displacement range ±15 mm), two glued vertically to measure shear displacement on either side of the specimen and two glued horizontally across to the steel plates on either end to measure rotation. Tests were stopped when a vertical displacement of 10 mm was measured in either of the joints to fully capture residual loads [77]. The testing apparatus (Fig. 9) uses two springs in parallel (axial stiffness $k = 115$ N/mm) to gradually accommodate volumetric changes in the specimen at increasing shear loads and keep the precompression level constant. Precompression loads were manually applied and monitored using a 300 kN hydraulic jack (Enerpac RCD3010) and 222 kN capacity load cell at 0.07% resolution. Failure modes were also recorded and compared to those listed in EN 1052–3 Annex A: shear failure in the unit-mortar interface (A.1), shear failure in the mortar (A.2), shear failure in the unit (A.3) and crushing in the units (A.4).

6.2. Shear test results

Most specimens exhibited shear failure in the mortar (A.2) or joint failure at the unit-mortar interface (A.1). At high precompression levels (e.g. 1.0 MPa) cracking through the full bricks at the height of the head joints was observed in a minority of the samples (see Fig. 9). Failure at the interface is commonly seen in tests on brick masonry with lime mortar [76,135] and tuff masonry with lime based mortar [136]. Differential failure within the mortar only occurred in the case of STP samples, at the interface of the cement repointing mortar and the original lime-based mortar.

Average shear strength values at each level of precompression (σ_{avg}), maximum shear force (F_v), maximum shear stress (τ_{max}), residual shear stress (τ_{res}) measured at the ultimate shear displacement and the strength degradation ratio (SDR) are summarized in Table 7. SDR is a measure of the ratio of residual shear stress to the maximum shear stress (SDR=τ_{res}/τ_{max}), a measurement of shear softening where higher SDR values indicate a lower degradation rate. SDR ranges from 0.74 to 0.94 in this work. Comparable triplet tests on lime mortar and clay brick tests from Segura et al. [76] report SDR between 0.67 – 0.90 while tests by Augenti and Parisi [136] for tuff masonry with lime mortar for confining stresses of 0.25, 0.5 and 0.75 MPa found SDR values between 0.63 – 0.80, and tests by Mirabella Roberti et al. [137] on mud brick triplets

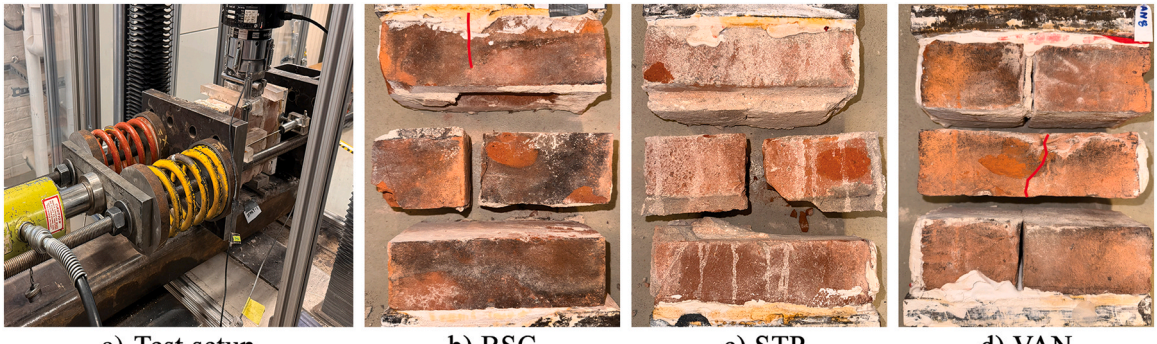

Fig. 9. Shear tests: a) setup and examples of recurrent failure modes b) A.2, c) A.1 and d) A.2.

Table 7
Overview of triplet shear test results at varying precompression levels.

Specimen type	σ_{avg} (MPa)	n	$F_{v,max}$ (kN)	τ_{max} (MPa)	COV (%)	τ_{res} (MPa)	COV (%)	SDR
BSC	0.19	1	8.52	0.21	-	0.16	-	0.74
	0.56	2	21.08	0.51	5.9	0.43	7.2	0.83
	0.97	1	22.12	0.56	-	0.48	-	0.85
STP	0.20	2	8.13	0.21	15.3	0.18	10.5	0.85
	0.62	2	18.88	0.50	21.6	0.41	7.9	0.82
	0.99	2	26.89	0.70	11.3	0.56	4.1	0.81
VAN	0.20	2	7.14	0.18	10.1	0.16	4.6	0.87
	0.59	2	16.40	0.42	7.1	0.38	5.4	0.91
	0.98	4	22.26	0.58	4.2	0.54	1.5	0.94

with hydraulic lime mortar for confining stresses of 0.12 and 1.25 MPa reported values between 0.51 and 0.69.

Shear stress is calculated using $F_v/2A$ where A is the area of the bed joint (mm^2) and shear displacement is the average of the vertical shear displacement of the mid-unit measured on either side of the specimen. Shear stress-displacement curves in Fig. 10 show a linear increasing curve at low levels of applied shear stress after which behaviour is nonlinear until peak load. After the peak load is reached, the curve either plateaus or decreases gradually until a residual stress is reached. The post-peak plateau represents inelastic frictional sliding after bond failure. This type of curve displays low levels of cohesion at the brick-mortar interface, whereas curves with high levels of cohesion exhibit a pronounced peak load followed by nonlinear softening, corresponding to progressive bond degradation [66]. Similar shapes of shear load and displacement curves were also seen in the three tests of field-extracted specimens by Atkinson et al. [44], described as weak and in a "disintegrated" state, where samples displayed nonlinear pre-peak behaviour and only one sample presented cohesive behaviour. Residual shear stress herein is calculated as an average of values in the residual range plateau region after a period of post-peak behaviour stabilization [138], a 7–29% decrease from the maximum where shear stress reaches a constant value. At each precompression level the results show an upward trend in maximum shear stress, consistent with the Mohr-Coulomb criterion and previous results from other researchers e.g. Augenti, Parisi [136,139,140]. 6–22% COV was presented at each precompression load, in line with triplet shear results of clay brick masonry [141,142]. VAN samples (Fig. 10, red) often had one joint which failed before the other, resulting in higher displacement at peak stress than other sites. No trend was observed related to which joint failed first. Failure of one joint prior to the other is a common phenomenon in the triplet shear test e.g. Alecci et al., [135], a noted difference from the couplet shear test which presents greater maximum stress values [76].

A linear regression analysis was completed assuming the well-accepted analogy with the Mohr-Coulomb failure criterion (Eq. 3). Values of bond cohesion c were interpreted as the intercept with the τ-axis and friction coefficient (μ) as the slope of the line, where friction angle (φ) is the arctangent of μ. Parameters are summarized for each building in Table 8 and all of the samples together, interpreted from the graphs presented in Fig. 11.

The linear regression curves present a coefficient of determination (R^2) between 0.76 and 0.96. Indeed, an $R^2 = 0.85$ for all samples (Fig. 11b) – despite variation in brick type, year constructed and masonry compressive strengths – portray a shear strength governed by the interface frictional properties. An overall friction coefficient of $\mu = 0.51$ in this work is lower than the values in the Eurocode ($\mu = 0.6$, Eq. 4) yet directly comparable to the Canadian standard ($\mu = 0.5$, Eq. 5). Considering similar tests on clay brick masonry and lime mortars, measured shear strengths, cohesion and friction angle values are comparable to e.g. Roberti et al., [53,76,135,137]. With respect to tests of field-extracted samples on old (and mechanically similar) masonry, Lumantarna et al. [8] (f_m=3.3 MPa and f_j=1.23 MPa) found a friction coefficient of 0.83 (48% difference) and cohesion of 0.15 MPa (14% difference). Replicated URM samples tested using analogous procedures by Touraille et al. [23] show higher shear strengths (0.2 – 1.8 MPa), friction coefficient (0.94) and cohesion (0.29 MPa) values. However, normal forces were not monitored and inflated values due to increased confinement and dilatancy (discussed later in this sub-section) might have affected

Table 8
Results from Mohr-Coulomb idealization from linear regression analysis related to URM shear tests.

Specimen type	n	Friction coefficient, μ	Cohesion, c (MPa)	R^2	Friction angle, φ (°)
BSC	4	0.44	0.20	0.76	23.9
STP	6	0.62	0.10	0.90	31.6
VAN	8	0.49	0.10	0.96	26.2
ALL	18	0.51	0.13	0.85	27.0

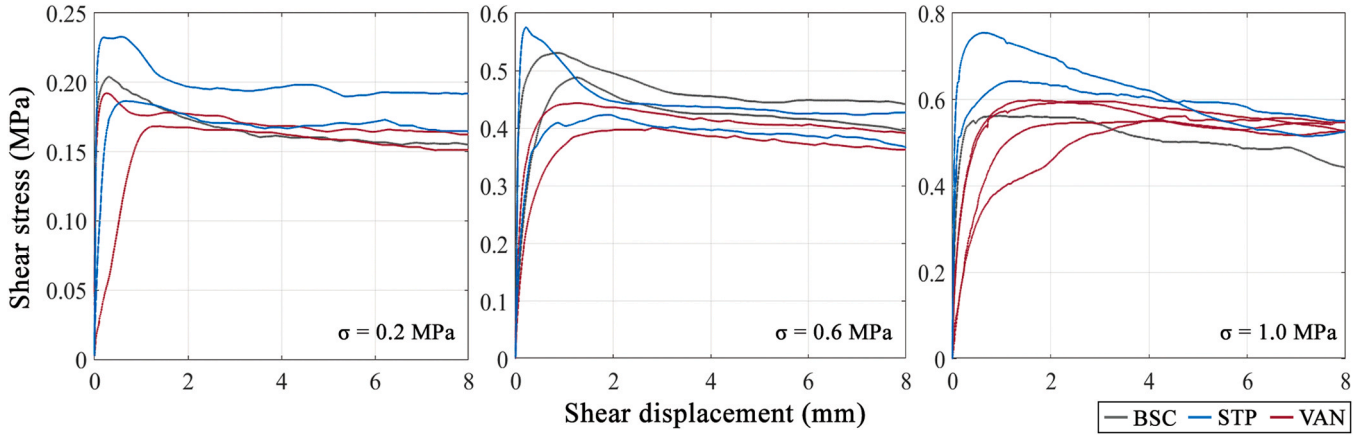

Fig. 10. Shear tests: stress vs displacement curves for each building type at three levels of precompression.

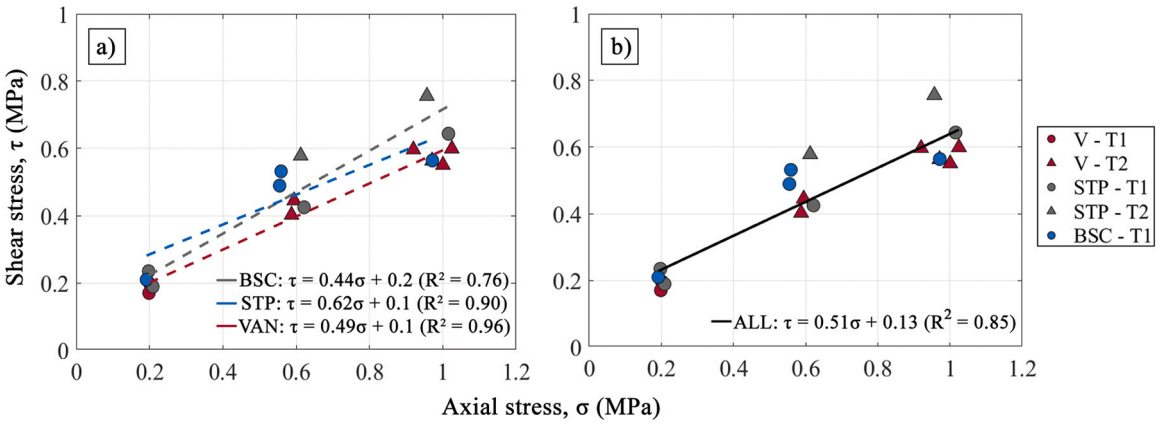

Fig. 11. Shear tests: (a) normal vs shear stress with linear regression curves for each URM type and (b) all samples.

measurements. Results fall within or below the range reported for similar materials, i.e. Briceño et al. [143], expected for field-extracted specimens.

Shear tests on field-extracted URM also provided further critical mechanical parameters. The shear modulus G_j is among those, herein measured as the slope of the shear stress and strain curve from 1/10–1/3 of the peak stress value as done by Jafari et al. [55]. Shear strain was taken as the relative shear displacement divided by the gage length of the installed LVDT. The shear modulus is herein referred to as G_j, being a measure of the deformability along the unit-mortar interface. The calculation of the fracture energy in shear (Mode II) is completed in this campaign using two methods. The first method, proposed Lourenço [144], calculates the cohesive fracture energy as the area under the curve of the shear stress and shear displacement curve above the residual shear stress (Fig. 6b). This value, referred to as $G_f{}^{II}$, is only valid for samples with identifiable peak shear stress and residual stress values. A second alternative method was proposed by Segura et al. [76], deemed to be better suited to the weak cohesive response of tested bonds, as those herein. This assumes the total area under the shear stress and displacement curve up to 2.5% strain, referred to as $G_{f\,2.5\%}^{II}$. Both fracture energy values and associated COVs are included in Table 9, where n refers to the number of samples.

The values of $G_f{}^{II}$ in Table 9 (0.05–0.49 Nmm/mm^2) are comparable to those reported in previous literature, if on the lower end, similar to those reported by Segura et al. [76] of 0.07–0.198 Nmm/mm^2 for clay bricks with lime mortar and 0.1 Nmm/mm^2 for calcium silicate masonry from a study completed by Augenti and Parisi [136]. These previous studies similarly show a linearly increasing $G_f{}^{II}$ with increasing levels of applied normal stress [55,76,136]. Comparing $G_{f\,2.5\%}^{II}$ (0.31–1.32 Nmm/mm^2) with results from Segura et al. [76] who reported values between 1.37 and 4.0 Nmm/mm^2, this study provides significantly lower estimates – approximately 3.16x lower.

Dilatancy (ψ), a mechanism of volumetric expansion [145], is measured as the slope of the normal displacement (Δv_{pl}) to shear displacement (Δu_{pl}) of the specimen in the plastic region of the curve, calculated in degrees based on the equation $\Delta\tan\psi = \frac{\Delta u_{pl}}{\Delta v_{pl}} * \omega$ where ω= 0.5 when both joints have failed. Dilatancy was calculated using the slope of the curve as the test progresses, as its magnitude tends towards zero when peak stress is reached [145,146]. Prior research shows the dilatancy angle is greatest in samples where the shear failure occurs within the mortar joint rather than at the unit-mortar interface, due to the expansion generated in the shear sliding within the mortar [139, 145]. Fig. 12 shows the relationship between normal and shear displacement, as well as the evolution of dilatancy with respect to shear loading.

In Fig. 12a, the curves exhibit a linear relationship between the normal and shear displacement which continues into the post peak region, also seen in Augenti and Parisi [136] and Segura et al. [76] but exaggerated in this work. Instead of dilatancy tending towards zero as the test continues after peak stress is reached, the field-extracted URM samples experience a non-zero level of dilatancy which is higher for greater levels of precompression, as can be seen in Fig. 12b. Research by [146,147] do not show the same trend. Indeed, the relationship between normal stress and dilatancy angle presented in Fig. 12c indicates a higher dilatancy angle measured just before the peak stress for higher levels of precompression, however a large scatter was present in this trendline (R^2=0.16). Research by [136,145,146] instead found diminished dilatancy at higher precompression levels. The different normal displacement behaviour of the field-extracted samples might be attributed to the presence of repointing along one surface of all joints, which may not have significant effect on the strength but instead on the uplift. Shear failure and continued crushing of mortar in friction along the cracking surface also plays a role, which can attribute to the higher dilatancy values after peak shear stress is reached, rather than simple debonding and sliding along the interface. Overall, the post-peak behaviour in the analysis of old masonry needs to be studied for

Table 9
Shear tests: shear moduli and fracture energy (Mode II).

Specimen type	σ_{avg} (MPa)	n	G_j (MPa)	COV (%)	G_f^{II} (Nmm/mm^2)	COV (%)	$G_{2.5\%}^{II}$ (Nmm/mm^2)	COV (%)
BSC	0.19	1	-	-	0.10	-	0.37	-
	0.56	2	502.2	99	0.24	27	0.92	9
	0.97	1	410.3	-	0.44	-	1.07	-
STP	0.20	2	181.2	52	0.05	0	0.39	11
	0.62	2	416.4	61	0.19	2	0.88	13
	0.99	2	1283.2	56	0.49	45	1.32	8
VAN	0.20	2	655.9	98	0.07	10	0.31	16
	0.59	2	185.6	39	0.14	17	0.54	52
	0.98	4	182.6	58	0.16	77	0.91	16
Average			477.15	66.12	0.20	26	0.79	18

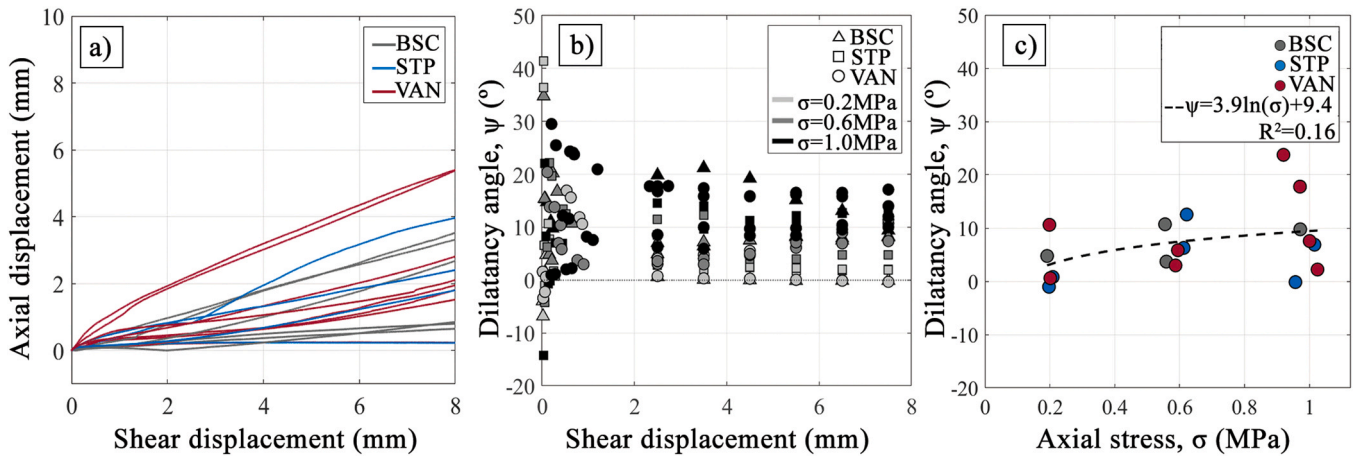

Fig. 12. a) Normal and shear displacement of each specimen, b) dilatancy angle and shear displacement, c) dilatancy angle measured as the slope between 85% and 95% of peak shear stress for each specimen and normal stress level.

further result verifications, as no prior tests on field-extracted masonry have reported fracture energy or dilatancy parameters.

7. Assessment and development of predictive equations

Reliable estimation of local material properties is essential for the structural and seismic assessment of existing buildings, particularly where site-specific characterization is limited. When destructive testing is not feasible, predictive equations offer a practical alternative for deriving mechanical properties from more accessible constituent parameters, such as unit and mortar strength. This section first benchmarks the experimental results against comparable masonry test programs, followed by an evaluation of available predictive equations and recommendations for mechanical property estimation. Table 10 summarizes the compressive properties of constituent materials and masonry assemblies obtained in this study, compared against three studies on replicated clay brick masonry conducted in Montréal, Canada and Georgia, USA. Tests by Yi et al. [148] included solid clay bricks and a lime based mortar (0.5:2:9, Portland cement:lime:sand), mimicking Type K mortar for lateral load tests of a two-storey building with timber diaphragms. No data was given on the material manufacturing. Paquette and Bruneau [149] conducted pseudo-dynamic tests of a single storey URM building with a timber diaphragm. Masonry included standard metric modular solid bricks and Type O mortar (1:2:9, cement:lime:sand). Liu et al. [92] utilized new moulded solid clay bricks (Glen-Gery 53DD Georgian) and a premixed Type O mortar (MasonMix Grey, Sika Canada Inc.) weakened with 15% additional sand in diagonal compression tests to evaluate a timber retrofit system.

Table 10 shows compressive strength results from this work are similar to or on the lower end of reported values for tests of replicated samples of clay brick masonry with lime-based mortar. Beyond strength parameters, the Young's modulus and shear modulus derived from compressive and shear tests can inform stiffness of masonry assemblies and components as a required design and assessment parameter. Design codes i.e. ([97,150]: TMS 402) recommend the ratio of shear modulus to the Young's modulus as $_{Gj/E} = 0.4$, yet other research has suggested this value is high for most masonry typologies [151], proposing ratios for $_{Gj/E}$ between 0.1 and 0.4 depending on the typology [151–153]. Table 11 presents experimentally derived $_{Gj/E}$ ratios from the compression and shear tests completed in this work. Values range from 0.2 to 0.5, with an average ratio of 0.4. Wilding et al. [151] proposed a G_j/E ratio of 0.3 for solid clay brick masonry with lime mortar and Petry and Beyer [152] proposed a G_j/E ratio of 0.25 for hollow clay brick and cement mortar, each lower than the average ratio of 0.4 derived from this work.

Further predictive models have been developed for the estimation of masonry compressive strength from mortar and brick strength, following the previously mentioned Eurocode 6 format of $f'_m = Kf_b^{\alpha} \times f_j^{\beta}$ (Eq. 1). Predictive equations have been since proposed for different masonry typologies, this work focuses on those for clay bricks with varying brick and mortar strengths, summarized in Table 12. Kaushik et al. [61] proposed an equation based on nonlinear regression analysis of experimental tests with low strength bricks (16–28 MPa) typical in Indian construction. Gumaste et al. [79] presents a comparison between the strength of prisms and wallets with two brick types and three types of cement and cement-lime mortars. Predictive equations were estimated for each using nonlinear regression. Costigan et al. [63] performed compression tests of frogged clay brick and lime and cement-lime mortars with varying strengths and curing times and proposed predictive models for the different mortar types using regression analysis. Lumantarna et al. [45] conducted a nonlinear regression analysis on experimental results from field-extracted and lab replicated masonry triplets of varying brick and mortar strengths to create a predictive model for existing masonry in New Zealand. Thamboo and Dhanasekar [154] evaluated brick masonry with a cement mortar in a comparison between compression tests of wallets and prisms, developing an analytical model for each using nonlinear regression. The higher values of α compared to β in the models of Table 12 display the stronger effect of the brick strength on the masonry strength. Only in the case of Costigan et al. [63] (Eq. 12), are the values for α and β similar.

These predictive models were leveraged to compare to the

Table 10
Comparison of field-extracted masonry to replicated samples tested in North America.

	this work	[148]	[149]	[23]	[92]
f_b (MPa)	28.92	41.6	109	26.30	70.60
f_j (MPa)	2.34	0.283	9.24	5.35	2.78
f_m (MPa)	7.5	10	22.2	14.80	17.50
Ratio f_b	-	1.44	3.77	0.91	2.44
Ratio f_j	-	0.12	3.95	2.29	1.19
Ratio f_m	-	1.33	2.96	1.97	2.33

Table 11
Values for the G/E ratio from measured masonry Young's modulus (E_m) and shear modulus (G_j).

Specimen type	Ratio f_b/f_j	E_m (MPa)	G_j (MPa)	G_j/E
BSC	7.7	2317.0	456.2	0.20
STP	28.9	1257.5	626.9	0.50
VAN	11.8	1321.5	341.4	0.26
Average	15.7	1200.0	477.2	0.40

Table 12
Summary of predictive equations for estimating the masonry compressive strength of URM assemblies.

Reference	Predictive equation	
Eurocode 6 [155]	$f'_m = 0.5 f_b^{0.7} \times f_j^{0.3}$	(9)
Kaushik et al. [61]	$f'_m = 0.63 f_b^{0.49} \times f_j^{0.32}$	(10)
Gumaste et al. [79]	$f'_m = 0.317 f_b^{0.866} \times f_j^{0.134}$	(11)
Costigan et al. [63]	$f'_m = 0.56 f_b^{0.53} \times f_j^{0.5}$	(12)
Lumantarna et al. [45]	$f'_m = 0.75 f_b^{0.75} \times f_j^{0.31}$	(13)
Thamboo and Dhanasekar [154]	$f'_m = 0.25 f_b^{1.26} \times f_j^{0.15}$	(14)

experimental values determined herein. Table 13 displays a summary of the experimentally determined strength of the brick, mortar and masonry for each masonry combination and the ratio of the experimental masonry strength to the predicted masonry strength calculated with each equation. Values lower than one overestimate strength while values greater than one underestimate strength. In this case, EC6 (Eq. 9) and Eq. 11 [79] present the best overall correlation between experimental and predicted values. However, none of the models were able to accurately represent compressive strength for all samples, especially considering outliers such as STP which has a high difference in brick to mortar strength, yet a lower masonry compressive strength.

An analytical model for the Eastern Canadian masonry types tested in this work was attempted using several statistical methods. Due to the relatively small sample size of five masonry types, which may not be representative of all combinations of brick/mortar strength combinations, statistical analysis for Eastern Canadian masonry did not agree upon distinct relevant parameters for an analytical model. Nonlinear regression (NREG) considering the three variables (K, α, β) was adopted in literature to create the models and was similarly implemented herein. As application of the nonlinear regression to the sites resulted in negative parameters, five alternative statistical methods were applied as alternative methods to calibrate the parameters including nonlinear least squares (NLS), log-transform linear regression (LOG), constrained regression with least square fit (CREG), minimization of the mean absolute percentage error (MAPE) and minimization of ratio bias. Cross validation was implemented to validate results. The CREG method sets $f'_m - K f_b^{\alpha} \times f_j^{\beta} = 0$ through the origin, and varies β in increasing iterations of 0.05 while K and α are determined by linear regression at each β to decrease the degrees of freedom of the regression analysis from three to two, where a minimum sum of square errors is calculated [63]. The R^2 and standard of error estimate (σ) are used to verify model fitness. Calculations of parameters are summarized in Table 14.

The statistical analyses displayed in Table 14 show limited correlation, indicated by negative R^2 values. The positive R^2 value for the nonlinear regression analysis and log-transform linear regression is related to a high K value and negative α and β parameters, showing a negative relationship between unit and mortar strengths. As the α and β parameters are directly related to the unit and mortar strengths, negative values cannot represent a realistic relationship with masonry compressive strength. Based on the statistical results from a building level analysis, a specimen level nonlinear regression analysis was completed to calibrate the same parameters of K, α and β. Inputs of brick, mortar and masonry compressive strength results described in the previous sections were used to calibrate the parameters for individual buildings. Table 15 presents the results of this analysis and can inform a recommend range of values for the parameters for use with local clay brick masonry typologies. Recommended K values range from 0.79 to 1.84, α values from 0.33 to 0.42 and β values from 0.43 to 0.51 can provide acceptable estimates of masonry strength when only the mortar and unit strengths are known. Considering average values of brick/mortar strengths and prediction coefficients from Table 15, the predicted masonry compressive strength is 6.68 MPa, 11% lower than the experimental average of 7.50 MPa.

Table 14
Masonry strength optimization summary.

Method	K	α	β	R^2	σ
EC6	0.50	0.70	0.30	-0.53	0.66
NREG	1054.1	-0.31	-4.90	0.48	0.41
NLS	2.00	0.31	0.34	-0.07	0.55
LOG	71.44	-0.11	-2.39	0.33	0.38
CREG	3.32	0.20	0.10	-0.02	0.55
Min. ratio	2.00	0.47	0.01	-0.60	0.41
Min. MAPE	0.77	0.26	1.40	-0.50	0.88

The calculated regression values capture general trends in the predictive equation, yet the variability inherent to existing masonry coupled with a relatively small sample size present challenges for a reliable analytical model. The range of brick strengths, low-strength lime mortars and the non-linear relationship between component and assembly strength suggest that further research is needed before a robust model can be established for Eastern Canadian masonry.

8. Conclusions

This study presents the first experimental characterization of field-extracted clay brick masonry constituents and assemblies from four typical 19th–20th century Eastern Canadian unreinforced masonry (URM) buildings with distinct original end uses. Results directly support a dataset of mechanical properties for Eastern Canadian old masonry, presently missing as values are currently only available from tests on replicated samples. This work includes compression tests on bricks and double punch tests on mortars, presenting physical, elastic and plastic properties. At the assembly scale, 59 URM samples were retrieved and uniaxial compression tests (ASTM C1314) under monotonic and cyclic

Table 15
Nonlinear regression analysis for masonry prediction coefficients based on individual building tests.

Specimen type	$f_{b,exp}$ (MPa)	$f_{j,exp}$ (MPa)	$f_{m,exp}$ (MPa)	K	α	β
BBE	11.5	2.69	5.7	1.16	0.40	0.50
BBL	26.9	2.03	14.1	1.84	0.42	0.51
BSC	17.3	2.25	4.2	0.79	0.36	0.43
STP	60.6	2.11	6.2	1.18	0.33	0.50
VAN	28.3	2.40	7.3	1.30	0.36	0.50
AVG	28.9	2.34	7.50	1.25	0.37	0.49

Table 13
Comparison of predictive models to experimental data.

Specimen type	$f_{b,exp}$ (MPa)	$f_{j,exp}$ (MPa)	$f_{m,exp}$ (MPa)	(Eq. 9) $f_{m,exp}$ / $f_{m,pred}$	(Eq. 10) $f_{m,exp}$ / $f_{m,pred}$	(Eq. 11) $f_{m,exp}$ / $f_{m,pred}$	(Eq. 12) $f_{m,exp}$ / $f_{m,pred}$	(Eq. 13) $f_{m,exp}$ / $f_{m,pred}$	(Eq. 14) $f_{m,exp}$ / $f_{m,pred}$
BBE	11.5	2.69	5.7	0.72	0.50	0.53	0.59	1.12	0.88
BBL	26.9	2.03	14.1	0.48	0.28	0.43	0.32	0.78	1.00
BSC	17.3	2.25	4.2	1.22	0.78	0.98	0.90	1.93	1.93
STP	60.6	2.11	6.2	1.96	0.96	1.98	1.16	3.31	6.36
VAN	28.3	2.40	7.3	1.02	0.59	0.88	0.70	1.65	2.11
Average	28.92	2.34	7	1.07	0.62	0.94	0.73	1.74	2.25

loading and direct shear (triplet) tests (EN 0152) were performed under three overburden pressures 0.2, 0.6, 1.0 MPa. The work is the first of its kind to show results from cyclic compression tests and analysis of fracture energy and dilatancy on field-extracted samples. The following conclusions can be drawn from this study:

- For the five types of clay brick masonry studied with different brick and mortar strengths, the masonry compressive strength (f_m=4.2–14.1, average 7.2 MPa) and Young's modulus (E_m=680–2740 MPa, average 1491 MPa) characteristics have provided consistent results for the distinct brick and mortar combinations. As with previous researchers, monotonic stress-strain curves were able to represent the peak cyclic behaviour.
- Compression and Mode II fracture energy values (17.3–65.2 N/mm and 0.1–0.5 Nmm/mm^2, respectively) are consistent with published ranges for comparable clay brick masonry with lime mortar. The wider scatter in Mode II fracture energy reflects the combined cohesive and frictional failure mechanisms at the bed joint interface and the direct dependency to applied precompression level.

Triplet shear tests present well aligned results across building sites and linear regression analysis, following the Mohr-Coulomb criterion, had an R^2= 0.85. Tests yielded shear modulus (G_j=341–626 MPa, average 477 MPa), friction coefficient (μ =0.4–0.7, average 0.5), dilatancy (1.3–30.6) and cohesion (c=0.1–0.2 MPa, average 0.13 MPa).

- This work also presents recommendations for design codes for the estimation of material properties, required for analysis and numerical models. The following predictive equations have been developed based on the experiments completed herein:
- Brick compressive strength to Young's modulus: E_b= 244*f_b (R^2=0.81).
- Masonry compressive strength to Young's modulus: E_m= 135* f_m (R^2=0.63).
- Shear-Young's modulus ratio of G_j/E = 0.4.
- For prediction of masonry compressive strength from brick and mortar strengths, using the equation format $f_m^{'} = Kf_b^{\alpha} \times f_j^{\beta}$ of Eurocode 6, the authors recommended K values between 0.8 and 1.8, α from 0.3 to 0.4 and β from 0.4 to 0.5.

The results provide a first look into the unique behaviour and characteristics of masonry when exposed to the conditions imposed by time, weather and craftmanship, previously undocumented for Eastern Canada. These findings constitute a foundational dataset for the mechanical characterization of extracted old masonry that, upon appropriate expansion and consolidation, will contribute to regional assessment practice, code development for existing buildings and calibration of nonlinear structural models. At present, the study's limitations include a reduced sample size due to site constraints. Expanding the dataset or complementing it with numerical models in a parametric manner would further support the development of reliable predictive solutions, something we are currently working towards.

CRediT authorship contribution statement

L. Davis: Writing – original draft, Visualization, Formal analysis, Data curation, Conceptualization. **W. Garcia Mendez:** Writing – review & editing, Investigation. **M.J. Nollet:** Writing – review & editing, Supervision. **D. Malomo:** Writing – review & editing, Supervision, Project administration, Funding acquisition, Conceptualization.

Declaration of Competing Interest

The authors declare that they have no known competing financial interests or personal relationships that could have appeared to influence the work reported in this paper

Acknowledgements

The authors acknowledge the support of the Natural Sciences and Engineering Research Council of Canada (NSERC) [funding reference number RGPIN-2022–03635] and the Fonds de recherche du Québec Nature et Technologies (FRQNT). The authors also wish to thank the Ville de Montréal for their time and generous support with access to building sites, material and onsite support, as well as Robert Hardy Inc. for their donation of materials and time in the extraction of the samples. We would also like to acknowledge the support of the Association des Entrepreneurs en Maçonnerie du Québec (AEMQ) and the Canadian Masonry Design Centre (CMDC) with special thanks to Adrien Sparling. R. Desbrousses, A. David, S. Løvfall Aasen, S. Palermo, S. Alahatabeh, R. Gallardo Davalos and M. El-Assaly are also gratefully acknowledged for their support in the experimental campaign. The first author is also grateful to the FRQNT-funded CEISCE (Centre d'études interuniversitaire des structures sous charges extrêmes) for additional scholarship funding received. We also wish to thank the two anonymous reviewers whose contributions have improved this manuscript.

Data availability

Data will be made available on request.

References

[1] L. Pelà, E. Canella, A. Aprile, P. Roca, Compression test of masonry core samples extracted from existing brickwork, Constr. Build. Mater. 119 (2016) 230–240, https://doi.org/10.1016/j.conbuildmat.2016.05.057.
[2] S. Petry, K. Beyer, Cyclic test data of six unreinforced masonry walls with different boundary conditions, Earthq. Spectra 31 (2015) 2459–2484, https://doi.org/10.1193/101513EQS269.
[3] G. Vasconcelos, P.B. Lourenço, In-plane experimental behavior of stone masonry walls under cyclic loading, J. Struct. Eng. 135 (2009) 1269–1277, https://doi.org/10.1061/(asce)st.1943-541x.0000053.
[4] S. Jafari, J.G. Rots, R. Esposito, A correlation study to support material characterisation of typical Dutch masonry structures, J. Build. Eng. 45 (2022) 103450, https://doi.org/10.1016/j.jobe.2021.103450.
[5] A. Simões, R. Bento, T.M. Ferreira, Mechanical properties of masonry structures in Portugal: proposal of new correlations with the Masonry Quality Index (MQI), Bull. Earthq. Eng. 24 (4) (2026) 2255–2277, https://doi.org/10.1007/s10518-026-02361-8. https://link.springer.com/10.1007/s10518-026-02361-8.
[6] D. Dizhur, J.M. Ingham, Diagonal tension strength of vintage unreinforced clay brick masonry wall panels, Constr. Build. Mater. 43 (2013) 418–427, https://doi.org/10.1016/j.conbuildmat.2013.02.015.
[7] D. Dizhur, R. Lumantarna, D.T. Biggs, J.M. Ingham, In-situ assessment of the physical and mechanical properties of vintage solid clay bricks, Mater. Struct. 2016 501 50 (2016) 63, https://doi.org/10.1617/S11527-016-0939-9.
[8] R. Lumantarna, D.T. Biggs, J.M. Ingham, Compressive, flexural bond, and shear bond strengths of in situ new zealand unreinforced clay brick masonry constructed using lime mortar between the 1880s and 1940s, J. Mater. Civ. Eng. 26 (2014) 559–566, https://doi.org/10.1061/(asce)mt.1943-5533.0000685.
[9] H. Kalman. A history of Canadian architecture, Oxford University Press, Don Mills, 1995.
[10] M. Yeheyis, K. Hewage, M.S. Alam, et al., An overview of construction and demolition waste management in Canada: a lifecycle analysis approach to sustainability, Clean. Technol. Environ. Policy 15 (2013) 81–91, https://doi.org/10.1007/s10098-012-0481-6.
[11] R. Fathi-Fazl, F. Fazileh, Z. Cai, Seismic Upgrading Guidelines (SUG) for existing buildings in Canada, Natl. Res. Counc. Can. (2025).
[12] D. Mitchell, R. Tinawi, T. Law. The 1988 Saguenay earthquake-A site visit report, 1989.
[13] M. Bruneau, M. Lamontagne, Damage from 20th century earthquakes in eastern Canada and seismic vulnerability of unreinforced masonry buildings, Can. J. Civ. Eng. 21 (4) (1994) 643–662, https://doi.org/10.1139/l94-065. http://www.nrcresearchpress.com/doi/10.1139/l94-065.
[14] A. Penna, C. Calderini, L. Sorrentino, et al., Damage to churches in the 2016 central Italy earthquakes, Bull. Earthq. Eng. 17 (2019) 5763–5790, https://doi.org/10.1007/s10518-019-00594-4.
[15] D. Dizhur, J. Ingham, L. Moon, et al., Performance of masonry buildings and churches in the 22 February 2011 Christchurch earthquake, Bull. New. Zeal Soc. Earthq. Eng. 44 (2011) 279–296, https://doi.org/10.5459/bnzsee.44.4.279-296.
[16] S. Lagomarsino, A. Penna, A. Galasco, S. Cattari, TREMURI program: an equivalent frame model for the nonlinear seismic analysis of masonry buildings,

Eng. Struct. 56 (2013) 1787–1799, https://doi.org/10.1016/j.engstruct.2013.08.002.
[17] M. Berti, L. Salvatori, M. Orlando, P. Spinelli, Unreinforced masonry walls with irregular opening layouts: reliability of equivalent-frame modelling for seismic vulnerability assessment, Bull. Earthq. Eng. 15 (2017) 1213–1239, https://doi.org/10.1007/s10518-016-9985-5.
[18] S. Bracchi, M. Rota, A. Penna, G. Magenes, Consideration of modelling uncertainties in the seismic assessment of masonry buildings by equivalent-frame approach, Bull. Earthq. Eng. 13 (2015), https://doi.org/10.1007/s10518-015-9760-z.
[19] M. Sorour, A. Elmenshawi, G. Parsekian, et al., An experimental programme for determining the characteristics of stone masonry walls, Can. J. Civ. Eng. 38 (2011) 1204–1215, https://doi.org/10.1139/l11-083.
[20] A. Elmenshawi, M. Sorour, D. Duchesne, et al., On the dynamic behaviour of strengthened stone masonry walls, Adv. Mater. Res. 133134 (2010) 671–676, https://doi.org/10.4028/www.scientific.net/AMR.133-134.671.
[21] A. Elmenshawi, M. Sorour, A. Mufti, et al., In-plane seismic behaviour of historic stone masonry, Can. J. Civ. Eng. 37 (2010) 465–476, https://doi.org/10.1139/L09-166.
[22] M.J. Nollet, L. Guizani, A. Abo El Ezz, et al., Experimental evaluation of the mechanical parameters for seismic assessment of traditional brick and stone masonry buildings in eastern Canada. Proceedings, Annual Conference - Canadian Society for Civil Engineering. Canadian Society for Civil Engineering, Laval, Canada, 2019.
[23] J. Touraille, M.-J. Nollet, A. Abo-El-Ezz, Experimental Investigation on the Lateral Strength of Unreinforced Brick Masonry Walls, 12th Can. Conf. Earthq. Eng. Que. City Can. (2019) 1–8.
[24] V. Alecci, G. Stipo, A. La Brusco, et al., Estimating elastic modulus of tuff and brick masonry: A comparison between on-site and laboratory tests, Constr. Build. Mater. 204 (2019) 828–838, https://doi.org/10.1016/j.conbuildmat.2019.01.224.
[25] S. Gonen, S. Soyoz, Investigations on the elasticity modulus of stone masonry, Structures 30 (2021) 378–389, https://doi.org/10.1016/j.istruc.2021.01.035.
[26] M. Uranjek, V. Bosiljkov, R. Žarnić, V. Bokan-Bosiljkov, In situ tests and seismic assessment of a stone-masonry building, Mater. Struct. Constr. 45 (2012) 861–879, https://doi.org/10.1617/s11527-011-9804-z.
[27] A. Borri, G. Castori, M. Corradi, E. Speranzini, Shear behavior of unreinforced and reinforced masonry panels subjected to in situ diagonal compression tests, Constr. Build. Mater. 25 (2011) 4403–4414, https://doi.org/10.1016/j.conbuildmat.2011.01.009.
[28] A. Brignola, S. Frumento, S. Lagomarsino, S. Podestá, Identification of shear parameters of masonry panels through the in-situ diagonal compression test, Int. J. Archit. Herit. 3 (2008) 52–73, https://doi.org/10.1080/15583050802138634.
[29] M. Corradi, A. Borri, A. Vignoli, Experimental study on the determination of strength of masonry walls, Constr. Build. Mater. 17 (2003) 325–337, https://doi.org/10.1016/S0950-0618(03)00007-2.
[30] I. Giongo, E. Rizzi, D. Riccadonna, M. Piazza, On-site testing of masonry shear walls strengthened with timber panels, Proc. Inst. Civ. Eng. Struct. Build. 174 (2021) 389–402, https://doi.org/10.1680/jstbu.19.00179.
[31] K.Q. Walsh, D.Y. Dizhur, J. Shafaei, et al., Situ out-of-plane testing of unreinforced masonry cavity walls in as-built and improved conditions, Structures 3 (2015) 187–199, https://doi.org/10.1016/j.istruc.2015.04.005.
[32] G. Vasconcelos, P.B. Lourenço, C.A.S. Alves, J. Pamplona, Ultrasonic evaluation of the physical and mechanical properties of granites, Ultrasonics 48 (2008) 453–466, https://doi.org/10.1016/j.ultras.2008.03.008.
[33] E. Vasanelli, D. Colangiuli, A. Calia, et al., Combining non-invasive techniques for reliable prediction of soft stone strength in historic masonries, Constr. Build. Mater. 146 (2017) 744–754, https://doi.org/10.1016/j.conbuildmat.2017.04.146.
[34] J. Thamboo, M. Corradi, K. Poologanathan, Investigating the mechanical characteristics of unreinforced and reinforced stone masonry using an experimental database, Bull. Earthq. Eng. (2024), https://doi.org/10.1007/s10518-023-01847-z.
[35] A. Borri, M. Corradi, G. Castori, A. De Maria, A method for the analysis and classification of historic masonry, Bull. Earthq. Eng. 13 (2015) 2647–2665, https://doi.org/10.1007/s10518-015-9731-4.
[36] F. Da Porto, M. Munari, A. Prota, C. Modena, Analysis and repair of clustered buildings: Case study of a block in the historic city centre of L'Aquila (Central Italy), Constr. Build. Mater. 38 (2013) 1221–1237, https://doi.org/10.1016/j.conbuildmat.2012.09.108.
[37] G.H. Nalon, J.C.L. Ribeiro, L.G. Pedroti, et al., Review of recent progress on the compressive behavior of masonry prisms, Constr. Build. Mater. 320 (2022) 126181, https://doi.org/10.1016/j.conbuildmat.2021.126181.
[38] L. Pelà, P. Roca, A. Benedetti, Mechanical characterization of historical masonry by core drilling and testing of cylindrical samples, Int. J. Archit. Herit. 10 (2016) 360–374, https://doi.org/10.1080/15583058.2015.1077906.
[39] E. Sassoni, C. Mazzotti, The use of small diameter cores for assessing the compressive strength of clay brick masonries, J. Cult. Herit. 14 (2013) e95–e101, https://doi.org/10.1016/j.culher.2012.11.027.
[40] A. Cabané, L. Pelà, P. Roca, Laboratory and in-situ mechanical characterisation of masonry components by comparing destructive and minor destructive testing techniques, Constr. Build. Mater. 411 (2024) 134474, https://doi.org/10.1016/j.conbuildmat.2023.134474.
[41] R.L.E. Desbrousses, L. Brickman, R.D. Gallardo, et al., Double-punch compressive resistance of Eastern Canada's low-strength mortars, J. Build. Eng. 112 (2025) 113910, https://doi.org/10.1016/j.jobe.2025.113910.
[42] L. Davis, D. Malomo, Experimental shear performance of old masonry walls typical of Eastern Canada, Constr. Build. Mater. 472 (2025) 140850, https://doi.org/10.1016/j.conbuildmat.2025.140850.
[43] J. Paquette, M. Bruneau, A. Filiatrault, Out-of-plane seismic evaluation and retrofit of turn-of-the-century north american masonry walls, J. Struct. Eng. 127 (2001) 561–569, https://doi.org/10.1061/(ASCE)0733-9445(2001)127:5(561).
[44] R.H. Atkinson, B.P. Amadei, S. Saeb, S. Sture, Response of masonry bed joints in direct shear, J. Struct. Eng. 115 (1989) 2276–2296, https://doi.org/10.1061/(asce)0733-9445(1989)115:9(2276).
[45] R. Lumantarna, D.T. Biggs, J.M. Ingham, Uniaxial Compressive Strength and Stiffness of Field-Extracted and Laboratory-Constructed Masonry Prisms, J. Mater. Civ. Eng. 26 (2014) 567–575, https://doi.org/10.1061/(asce)mt.1943-5533.0000731.
[46] M. Ispir, A. Ilki, Behavior of historical unreinforced brick masonry walls under monotonic and cyclic compression, Arab. J. Sci. Eng. 38 (2013) 1993–2007, https://doi.org/10.1007/s13369-013-0567-4.
[47] D. Ucer, A. Ulybin, S. Zubkov, S.T. Elias-Ozkan, Analysis on the mechanical properties of historical brick masonry after machinery demolition, Constr. Build. Mater. 161 (2018) 186–195, https://doi.org/10.1016/j.conbuildmat.2017.11.090.
[48] E. Sassoni, C. Mazzotti, G. Pagliai, Comparison between experimental methods for evaluating the compressive strength of existing masonry buildings, Constr. Build. Mater. 68 (2014) 206–219, https://doi.org/10.1016/j.conbuildmat.2014.06.070.
[49] F. Ferretti, B. Ferracuti, C. Mazzotti, M. Savoia, Destructive and minor destructive tests on masonry buildings: experimental results and comparison between shear failure criteria, Constr. Build. Mater. 199 (2019), https://doi.org/10.1016/j.conbuildmat.2018.11.246.
[50] C. Mazzotti, E. Sassoni, G. Pagliai, Determination of shear strength of historic masonries by moderately destructive testing of masonry cores, Constr. Build. Mater. 54 (2014) 421–431, https://doi.org/10.1016/j.conbuildmat.2013.12.039.
[51] J. Segura, L. Pelà, P. Roca, A. Cabané, Experimental analysis of the size effect on the compressive behaviour of cylindrical samples core-drilled from existing brick masonry, Constr. Build. Mater. 228 (2019), https://doi.org/10.1016/j.conbuildmat.2019.116759.
[52] L. Pelà, S. Saloustros, P. Roca, Cylindrical samples of brick masonry with aerial lime mortar under compression: Experimental and numerical study, Constr. Build. Mater. 227 (2019) 11–13, https://doi.org/10.1016/j.conbuildmat.2019.116782.
[53] L. Pelà, K. Kasioumi, P. Roca, Experimental evaluation of the shear strength of aerial lime mortar brickwork by standard tests on triplets and non-standard tests on core samples, Eng. Struct. 136 (2017) 441–453, https://doi.org/10.1016/j.engstruct.2017.01.028.
[54] S. Jafari, J.G. Rots, R. Esposito, Core testing method to assess nonlinear behavior of brick masonry under compression: a comparative experimental study, Constr. Build. Mater. 218 (2019) 193–205, https://doi.org/10.1016/j.conbuildmat.2019.04.188.
[55] S. Jafari, J.G. Rots, R. Esposito, Core testing method to assess nonlinear shear-sliding behaviour of brick-mortar interfaces: a comparative experimental study, Constr. Build. Mater. 244 (2020) 118236, https://doi.org/10.1016/j.conbuildmat.2020.118236.
[56] U. Jain, R. Esposito, Mechanical Characterisation of Multi-wythe Quay Walls in Amsterdam, Int. Conf. Struct. Anal. Hist. Constr. (2025) 554–567.
[57] J. Dorji, T. Zahra, D. Thambiratnam, D. Lee, Strength assessment of old masonry arch bridges through moderate destructive testing methods, Constr. Build. Mater. 278 (2021), https://doi.org/10.1016/j.conbuildmat.2021.122391.
[58] P.B. Lourenço, J.G. Rots, Multisurface Interface Model for Analysis of Masonry Structures, J. Eng. Mech. 123 (1997) 660–668, https://doi.org/10.1061/(asce)0733-9399(1997)123:7(660).
[59] L. Binda, A. Saisi, C. Tiraboschi, Investigation procedures for the diagnosis of historic masonries, Constr. Build. Mater. 14 (2000) 199–233, https://doi.org/10.1016/S0950-0618(00)00018-0.
[60] R.G. Drysdale, A.A. Hamid, L.R. Baker, Masonry Structures: Behaviour and Design, 3rd edition, Can. Mason. Des. Cent. 769 (1999).
[61] H.B. Kaushik, D.C. Rai, S.K. Jain, Stress-Strain Characteristics of Clay Brick Masonry under Uniaxial Compression, J. Mater. Civ. Eng. 19 (2007) 728–739, https://doi.org/10.1061/(asce)0899-1561(2007)19:9(728).
[62] E. Vintzileou, A. Miltiadou-Fezans, Mechanical properties of three-leaf stone masonry grouted with ternary or hydraulic lime-based grouts, Eng. Struct. 30 (2008) 2265–2276, https://doi.org/10.1016/j.engstruct.2007.11.003.
[63] A. Costigan, S. Pavía, O. Kinnane, An experimental evaluation of prediction models for the mechanical behavior of unreinforced, lime-mortar masonry under compression, J. Build. Eng. 4 (2015) 283–294, https://doi.org/10.1016/j.jobe.2015.10.001.
[64] A. Drougkas, P. Roca, C. Molins, Compressive strength and elasticity of pure lime mortar masonry, Mater. Struct. Constr. 49 (2016) 983–999, https://doi.org/10.1617/s11527-015-0553-2.
[65] G. Mohamad, F.S. Fonseca, A.T. Vermeltfoort, et al., Strength, behavior, and failure mode of hollow concrete masonry constructed with mortars of different strengths, Constr. Build. Mater. 134 (2017) 489–496, https://doi.org/10.1016/j.conbuildmat.2016.12.112.
[66] G. Vasconcelos, P.B. Lourenço, Experimental characterization of stone masonry in shear and compression, Constr. Build. Mater. 23 (2009) 3337–3345, https://doi.org/10.1016/j.conbuildmat.2009.06.045.
[67] G. Vasconcelos, P.B. Lourenço, C.A.S. Alves, J. Pamplona, Compressive Behavior of Granite: Experimental Approach, J. Mater. Civ. Eng. 21 (2009) 502–511, https://doi.org/10.1061/(ASCE)0899-1561(2009)21:9(502).

[68] C. Almeida, J.P. Guedes, A. Arêde, et al., Physical characterization and compression tests of one leaf stone masonry walls, Constr. Build. Mater. 30 (2012) 188–197, https://doi.org/10.1016/J.CONBUILDMAT.2011.11.043.

[69] O. Amer, D. Aita, D.V. Bompa, et al., Behavior of unreinforced multi-leaf stone masonry walls under axial compression: Experimental and numerical investigation, Eng. Struct. 293 (2023) 116621, https://doi.org/10.1016/J.ENGSTRUCT.2023.116621.

[70] A.R. AbdAllah, B. AbdelRahman, K. Galal, Influence of material properties and reinforcement on the compressive and shear strengths of concrete masonry: An experimental study, Structures 78 (2025) 108936, https://doi.org/10.1016/j.istruc.2025.108936.

[71] K.C. Voon, J.M. Ingham, Experimental In-Plane Shear Strength Investigation of Reinforced Concrete Masonry Walls, J. Struct. Eng. 132 (2006) 400–408, https://doi.org/10.1061/(ASCE)0733-9445(2006)132:3(400).

[72] R.G. Drysdale, A.A. Hamid, Behavior of Concrete Block Masonry Under Axial Compression, Acids J. Proc. 76 (1979), https://doi.org/10.14359/6965.

[73] F.M. Khalaf, Factors influencing compressive strength of concrete masonry prisms, Mag. Concr. Res. 48 (1996) 95–101, https://doi.org/10.1680/MACR.1996.48.175.95.

[74] G. Mohamad, P.B. Lourenço, H.R. Roman, Mechanics of hollow concrete block masonry prisms under compression: Review and prospects, Cem. Concr. Compos. 29 (2007) 181–192, https://doi.org/10.1016/J.CEMCONCOMP.2006.11.003.

[75] K. Naraine, S. Sinha, Behavior of Brick Masonry Under Cyclic Compressive Loading, J. Struct. Eng. 115 (1989) 1432–1445, https://doi.org/10.1061/(asce)0733-9445(1989)115:6(1432).

[76] J. Segura, E. Bernat, V. Mendizábal, et al., Experimental comparison of two testing setups for characterizing the shear mechanical properties of masonry, J. Build. Eng. 44 (2021) 103277, https://doi.org/10.1016/j.jobe.2021.103277.

[77] L. Binda, C. Tiraboschi, G. Mirabella Roberti, et al., Experimental and numerical investigation on a brick masonry building prototype-Report 5.0-Measuring masonry materials properties: Detailed results from an extensive experimental research, CNR - Grup. Naz. per la Dif. dai Terre - Rep. 51 (1996).

[78] C.T. Grimm, Strength and related properties of brick masonry, ASCE J. Struct. Div. 101 (1975) 217–232, https://doi.org/10.1061/jsdeag.0003970.

[79] K.S. Gumaste, K.S.N. Rao, B.V.V. Reddy, K.S. Jagadish, Strength and elasticity of brick masonry prisms and wallettes under compression, Mater. Struct. Constr. 40 (2007) 241–253, https://doi.org/10.1617/s11527-006-9141-9.

[80] H.B. Kaushik, D.C. Rai, S.K. Jain, Uniaxial compressive stress-strain model for clay brick masonry, Curr. Sci. 92 (2007) 497–501.

[81] C. Turco, M.O. Teixeira, E. Teixeira, R. Mateus, Mechanical properties and durability of compressed earth blocks incorporating natural materials, J. Build. Eng. 111 (2025), https://doi.org/10.1016/j.jobe.2025.113386.

[82] F. Wu, G. Li, H.N. Li, J.Q. Jia, Strength and stress-strain characteristics of traditional adobe block and masonry, Mater. Struct. Constr. 46 (2013), https://doi.org/10.1617/s11527-012-9987-y.

[83] L. Miccoli, U. Müller, P. Fontana, Mechanical behaviour of earthen materials: A comparison between earth block masonry, rammed earth and cob, Constr. Build. Mater. 61 (2014) 327–339, https://doi.org/10.1016/j.conbuildmat.2014.03.009.

[84] V. Nikolopoulou, C.E. Adami, D. Karagiannaki, et al., Grouts for strengthening two- and three-leaf stone masonry, made with earthen mortars, Int. J. Archit. Herit. 13 (2019), https://doi.org/10.1080/15583058.2018.1463414.

[85] Y. Endo, K. Yamaguchi, T. Hanazato, C. Mishra, Characterisation of mechanical behaviour of masonry composed of fired bricks and earthen mortar, Eng. Fail. Anal. 109 (2020), https://doi.org/10.1016/j.engfailanal.2019.104280.

[86] W.S. McNary, D.P. Abrams, Mechanics of Masonry in Compression, J. Struct. Eng. 111 (1985) 857–870, https://doi.org/10.1061/(ASCE)0733-9445(1985)111:4(857).

[87] A. Soleymani, M.A. Najafgholipour, A. Johari, An experimental study on the mechanical properties of solid clay brick masonry with traditional mortars, J. Build. Eng. 58 (2022) 105057, https://doi.org/10.1016/j.jobe.2022.105057.

[88] B. Liang, H. Zhang, Z. Liu, J. Hou, The influence of different types of mortar on the compressive strength of masonry, J. Build. Eng. 65 (2023) 105635, https://doi.org/10.1016/j.jobe.2022.105635.

[89] A.H. Salmanpour, N. Mojsilovic, J. Schwartz, Deformation capacity of unreinforced masonry walls subjected to in-plane loading: a state-of-the-art review, Int. J. Adv. Struct. Eng. 5 (2013).

[90] G. Magenes, G.M. Calvi, In-plane seismic response of brick masonry walls, Earthq. Eng. Struct. Dyn. 26 (1997) 1091–1112, https://doi.org/10.1002/(SICI)1096-9845(199711)26:11<1091::AID-EQE693>3.0.CO;2-6.

[91] L. Garcia-Ramonda, L. Pelá, P. Roca, G. Camata, In-plane shear behaviour by diagonal compression testing of brick masonry walls strengthened with basalt and steel textile reinforced mortars, Constr. Build. Mater. 240 (2020) 117905, https://doi.org/10.1016/j.conbuildmat.2019.117905.

[92] J. Liu, M. El-Assaly, W. Garcia Mendez, et al., A low-cost timber cladding system for the sustainable retrofit of masonry buildings: mechanical characterization under diagonal compression, Eng. Struct. 322 (2025) 119099, https://doi.org/10.1016/J.ENGSTRUCT.2024.119099.

[93] N. Mojsilović, Strength of masonry subjected to in-plane loading: A contribution, Int. J. Solids Struct. 48 (2011) 865–873, https://doi.org/10.1016/J.IJSOLSTR.2010.11.019.

[94] S. Kallioras, F. Graziotti, A. Penna, Numerical assessment of the dynamic response of a URM terraced house exposed to induced seismicity, Bull. Earthq. Eng. 17 (2019) 1521–1552, https://doi.org/10.1007/s10518-018-0495-5.

[95] F. Ferretti, S. Jafari, R. Esposito, et al., Critical analysis on the use of the shove test for investigating the shear-sliding behavior of brick masonry, Eng. Struct. 254 (2022) 113860, https://doi.org/10.1016/j.engstruct.2022.113860.

[96] A. Armanasco, D. Foppoli, A flat jacks method for in situ testing of brick masonry shear characteristics, Constr. Build. Mater. 262 (2020) 119840, https://doi.org/10.1016/j.conbuildmat.2020.119840.

[97] NZSEE (2017) New Zealand Society for Earthquake Engineering, Structural Engineering Society New Zealand Inc. (SESOC), New Zealand Geotechnical Society Inc., Ministry of Business, Innovation and Employment, Earthquake Commission. The Seismic Assessment of Existing Buil.

[98] D. Malomo, Y. Xie, G. Doudak, Unified life-cycle cost–benefit analysis framework and critical review for sustainable retrofit of Canada's existing buildings using mass timber, Can. J. Civ. Eng. (2023), https://doi.org/10.1139/cjce-2023-0222.

[99] L. Davis, D. Malomo, Structural characterization of Eastern Canada's old industrial masonry buildings via typological analysis: part II – building database analysis, Proc. Inst. Civ. Eng. - Eng. Hist. Herit. (2024), https://doi.org/10.1680/jenhh.24.00011.

[100] L. Davis, D. Malomo, Geometrical and Material Characterization of Old Industrial Masonry Buildings in Eastern Canada. Proceedings of the Canadian Society for Civil Engineering Annual Conference, Springer Science and Business Media Deutschland GmbH, 2024, pp. 351–364.

[101] R. Neill, Canal Era Ind. Can. 1791-1840. Univ. Prince Edw. Isl. Carlet. Univ. (2003).

[102] D. Bliek, P. Gauthier, Understanding the built form of industrialization along the Lachine Canal in Montreal, Urban. Hist. Rev. 35 (2006) 3–17, https://doi.org/10.7202/1015990ar.

[103] J.-C. Marsan, Montreal in Evolution: Historical Analysis of the Development of Montreal's Architecture and Urban Environment, McGill-Queen's University Press, Montreal, 1990.

[104] A. Grenier, Incendies et pompiers à Québec, 1640-2001, Éditions GID (2005).

[105] T. Ritchie, Bricks, Can. Build. Dig. (1974) 1–5, https://doi.org/10.4224/40000701.

[106] T. Ritchie, Developments in brick manufacture and use, Can. Clay Ceram. 51 (8) (1978).

[107] B.A. Humphreys, M. Sykes, The buildings of Canada, Read. 'S. Dig. Assoc. Can. (1980).

[108] B. Magrill, An Architecture of the Printed Page: Canada's Consumption of Pattern Books and Journals in Late Nineteenth-century Church-building, J. Soc. Study Archit. Can. 33 (2008) 33–42.

[109] A.B. McCullough, View of Technology and Textile Mill Architecture in Canada, Mater. Cult. Rev. 30 (1989).

[110] F.E. Kidder, H. Parker, Kidder-Parker architects' and builders' handbooks, J. Wiley & Sons, Inc, 1936.

[111] L. Davis, D. Malomo, Structural characterization of Eastern Canada's old industrial masonry buildings via typological analysis: part I – construction technologies through time, Proc. Inst. Civ. Eng. - Eng. Hist. Herit. (2024), https://doi.org/10.1680/jenhh.24.00010.

[112] F. Caron, ÉNon é De. l'Int. éR. êt Patrim. De. l'Anc. Casern. St. -Gabriel (2014).

[113] O. Paré, L'hôtel de ville de Sainte-Cunégonde. In: Encycl. du MEM, 2017https://ville.montreal.qc.ca/memoiresdesmontrealais/lhotel-de-ville-de-sainte-cunegondeAccessed 20 Nov 2025.

[114] D. Friedman, The Structure of Skyscrapers in America, 1871–1900: Their History and Preservation, Association for Preservation Technology, Springfield, 2020.

[115] A. Cabané, L. Pelà, P. Roca, Effect of cross section aspect ratio and bearing surfaces treatment on the compressive strength of solid fired clay brick specimens, Constr. Build. Mater. 383 (2023) 131397, https://doi.org/10.1016/j.conbuildmat.2023.131397.

[116] C.L. Khoo, A.W. Hendry, Strength tests on brick and mortar under complex stresses for the development of a failure criterion for brickwork in compression, Proc. Br. Ceram. Soc. (1973) 51–66.

[117] D. Łątka, Prediction of Mortar Compressive Strength Based on Modern Minor-Destructive Tests, Mater. (Basel) 16 (2023), https://doi.org/10.3390/ma16062402.

[118] A. Benedetti, M. Tarozzi, Interpretation formulas for in situ characterization of mortar strength, Constr. Build. Mater. 242 (2020) 118093, https://doi.org/10.1016/J.CONBUILDMAT.2020.118093.

[119] D. Łatka, P. Matysek, Determination of Mortar Strength in Historical Brick Masonry Using the Penetrometer Test and Double Punch Test, 13:2873, Mater 2020 13 (2020) 2873, https://doi.org/10.3390/MA13122873.

[120] H. Sugo, A.W. Page, S. Lawrence, Influ. age Mason. Bond. Strength. Mortar Microstruct. 34 (2007) 1433–1442, https://doi.org/10.1139/L07-137, https://doi.org/101139/L07-137.

[121] J. Segura, L. Pelà, P. Roca, Monotonic and cyclic testing of clay brick and lime mortar masonry in compression, Constr. Build. Mater. 193 (2018) 453–466, https://doi.org/10.1016/j.conbuildmat.2018.10.198.

[122] L. Binda, C. Tiraboschi, G. Mirabella, et al., GNDT_REP (1996), 5-1_1996_part II 2.pdf.

[123] S. Jafari, R. Esposito, S. Jafari. Material tests for the characterisation of replicated calcium silicate brick masonry, Delft University of Technology, 2016.

[124] P.B. Lourenço, J.G. Rots, J. Blaauwendraad, Continuum model for masonry: parameter estimation and validation, J. Struct. Eng. 124 (1998) 642–652, https://doi.org/10.1061/(asce)0733-9445(1998)124:6(642).

[125] E. Cuadros-Rojas, L. Garcia-Ramonda, P. Roca, L. Pelà, Experimental analysis of the compressive behaviour of perforated brick masonry using digital image correlation, Constr. Build. Mater. 431 (2024) 136471, https://doi.org/10.1016/j.conbuildmat.2024.136471.

[126] N. Augenti, F. Parisi, Constitutive Models for Tuff Masonry under Uniaxial Compression, J. Mater. Civ. Eng. 22 (2010) 1102–1111, https://doi.org/10.1061/(ASCE)MT.1943-5533.0000119.

[127] S. Jafari, R. Esposito. Material Characterisation of Existing Masonry for URM Abacus, Delft University of Technology, 2018.
[128] I. Bello, F. Martínez-Abella, G. Wardeh, B. González-Fonteboa, Complete stress-strain analysis of masonry prisms under compressive loading-unloading cycles through digital image correlation, Eng. Struct. 298 (2024), https://doi.org/10.1016/j.engstruct.2023.117088.
[129] L. Facconi, F. Minelli, F.J. Vecchio, Predicting uniaxial cyclic compressive behavior of brick masonry: new analytical model, J. Struct. Eng. 144 (2018) 04017213, https://doi.org/10.1061/(asce)st.1943-541x.0001961.
[130] D.V. Oliveira, P.B. Lourenço, P. Roca, Cyclic behaviour of stone and brick masonry under uniaxial compressive loading, Mater. Struct. 39 (2006) 247–257, https://doi.org/10.1617/s11527-005-9050-3.
[131] G. De Felice, Load-carrying capacity of multi-span masonry arch bridges having limited ductility, in: E. Fodde (Ed.), Structural Analysis of Historic Construction: Preserving Safety and Significance - Proceedings of the 6th International Conference on Structural Analysis of Historic Construction, SAHC08, CRC Press, 2008, pp. 541–546.
[132] A. Hsieh, A.V. Dyskin, P. Dight, The increase in Young's modulus of rocks under uniaxial compression, Int. J. Rock. Mech. Min. Sci. 70 (2014), https://doi.org/10.1016/j.ijrmms.2014.05.009.
[133] B. Yao, X. Zhang, W. Yang, et al., Time-dependent mechanical properties of red sandstone under fatigue-creep interaction loading, Rock. Mech. Rock. Eng. 58 (2025), https://doi.org/10.1007/s00603-025-04642-1.
[134] J. Thamboo, J. Bandara, S. Perera, et al., Experimental and analytical study of masonry subjected to uniaxial cyclic compression, Mater. (Basel) 13 (2020) 1–17, https://doi.org/10.3390/ma13204505.
[135] V. Alecci, M. Fagone, T. Rotunno, M. De Stefano, Shear strength of brick masonry walls assembled with different types of mortar, Constr. Build. Mater. 40 (2012) 1038–1045, https://doi.org/10.1016/j.conbuildmat.2012.11.107.
[136] N. Augenti, F. Parisi, Constitutive modelling of tuff masonry in direct shear, Constr. Build. Mater. 25 (2011) 1612–1620, https://doi.org/10.1016/j.conbuildmat.2010.10.002.
[137] G.M. Roberti, L. Binda, G. Cardani, Numerical modeling of shear bond tests on small brick-masonry assemblages, in: G.N. Pande, J. Middleton, B. Kralj CP (Eds.), Computer Methods in Structural Masonry, 4, 1997, pp. 144–153.
[138] L.J. Gooch, M.J. Masia, M.G. Stewart, M. Spadari, Experimental characterisation of the friction coefficient of mortar bed joints in clay-brick masonry, Constr. Build. Mater. 489 (2025) 142348, https://doi.org/10.1016/J.CONBUILDMAT.2025.142348.
[139] G. Andreotti, F. Graziotti, G. Magenes, Detailed micro-modelling of the direct shear tests of brick masonry specimens: the role of dilatancy, Eng. Struct. 168 (2018) 929–949, https://doi.org/10.1016/j.engstruct.2018.05.019.
[140] M. Angelillo, P.B. Lourenço, G. Milani, Masonry behaviour and modelling, CISM Int. Cent. Mech. Sci. Courses Lect. (2014) 1–26.
[141] D.V. Bompa, A.Y. Elghazouli, Experimental and numerical assessment of the shear behaviour of lime mortar clay brick masonry triplets, Constr. Build. Mater. 262 (2020) 120571, https://doi.org/10.1016/j.conbuildmat.2020.120571.
[142] L.J. Gooch, M.J. Masia, M.G. Stewart, C.Y. Lam, Statistical assessment of tensile and shear properties of unreinforced clay brick masonry, Constr. Build. Mater. 386 (2023) 131578, https://doi.org/10.1016/J.CONBUILDMAT.2023.131578.
[143] C. Briceño, M. Azenha, G. Vasconcelos, P.B. Lourenço, Influence of conditioning of clay bricks over shear strength of brick masonry, J. Build. Eng. 82 (2024) 108138, https://doi.org/10.1016/j.jobe.2023.108138.
[144] P.B. Lourenço, Computational Strategies for Masonry Structures, Delft University of Technology, 1996.
[145] G. Andreotti, F. Graziotti, G. Magenes, Expansion of mortar joints in direct shear tests of masonry samples: implications on shear strength and experimental characterization of dilatancy, Mater. Struct. 52 (2019), https://doi.org/10.1617/s11527-019-1366-5.
[146] R. van der Pluijm. Out-of-Plane Bending of Masonry Behaviour and Strength, 1999.
[147] G.P.A.G. van Zijl, Modeling masonry shear-compression: role of dilatancy highlighted, J. Eng. Mech. 130 (2004) 1289–1296, https://doi.org/10.1061/(asce)0733-9399(2004)130:11(1289).
[148] T. Yi, F.L. Moon, R.T. Leon, L.F. Kahn, Lateral load tests on a two-story unreinforced masonry building, J. Struct. Eng. 132 (2006) 643–652, https://doi.org/10.1061/(asce)0733-9445(2006)132:5(643).
[149] J. Paquette, M. Bruneau, Pseudo-dynamic testing of unreinforced masonry buildings with flexible diaphragm, J. Struct. Eng. 129 (2003) 1–7, https://doi.org/10.1061/(ASCE)0733-9445(2003)129:6(708).
[150] CEN, Eurocode 6 - Design of masonry structures, 2005.
[151] B.V. Wilding, M. Godio, K. Beyer, The ratio of shear to elastic modulus of in-plane loaded masonry, Mater. Struct. Constr. 53 (2020), https://doi.org/10.1617/s11527-020-01464-1.
[152] S. Petry, K. Beyer, Force-displacement response of in-plane-loaded URM walls with a dominating flexural mode, Earthq. Eng. Struct. Dyn. 44 (2015), https://doi.org/10.1002/eqe.2597.
[153] M. Tomaževič, Shear resistance of masonry walls and Eurocode 6: shear versus tensile strength of masonry, Mater. Struct. 42 (2009) 889–907, https://doi.org/10.1617/s11527-008-9430-6.
[154] J.A. Thamboo, M. Dhanasekar, Correlation between the performance of solid masonry prisms and wallettes under compression, J. Build. Eng. 22 (2019) 429–438, https://doi.org/10.1016/j.jobe.2019.01.007.
[155] BSI, Design of masonry structures - Part 1-1: General rules for reinforced and unreinforced masonry structures, Eur. 6 BS EN 1996 (2005) 123.